Charles University in Prague
Faculty of Mathematics and Physics

DIPLOMA THESIS

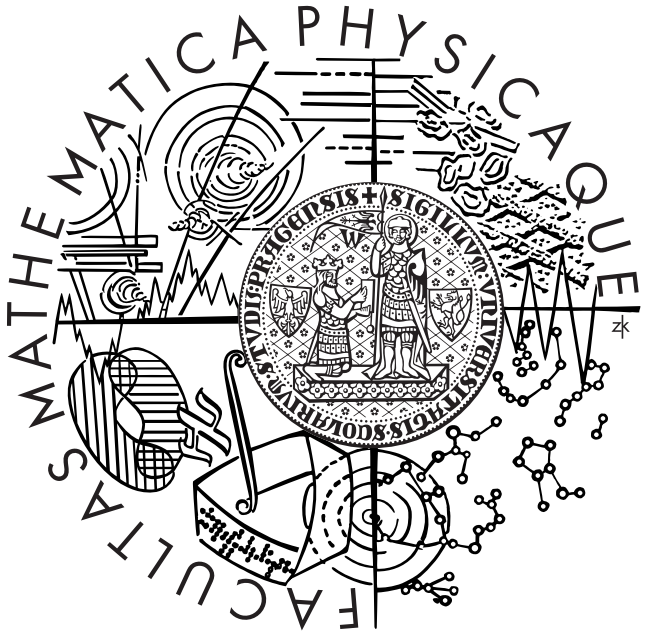

Jan Pipek

The Measurement of Top Quark Mass in Proton–Proton Collisions in the ATLAS Detector

Study Programme: Physics, Particle and Nuclear Physics
Supervisor: RNDr. Jiří Chudoba, PhD.
Institute of Physics, AS CR

Acknowledgement

I would like to thank all the people that supported me during my studies, first and foremost my parents and the supervisor of this work. Further Jan Kapitán should not be left aside for his invaluable help with ROOT, Vít Gottwald because of giving advice on many aspects of using the LaTeX typesetting system, to Karel Smolek for answering many of my top quark related questions and last but not least my thanks belong to Martin Kapoun, my high-school teacher who led my steps towards the investigation of nature.

Prohlašuji, že jsem svou diplomovou práci napsal samostatně a výhradně s použitím citovaných pramenů. Souhlasím se zapůjčováním práce.

I declare that I have completed the diploma thesis myself and used only the mentioned literature. I agree with using this diploma thesis freely.

Prague, 10$^{\text{th}}$ January 2006

Contents

Název práce: *Měření hmoty top kvarku v proton–protonových srážkách v detektoru ATLAS*
Autor: *Jan Pipek*
Katedra: *Ústav částicové a jaderné fyziky*
Vedoucí diplomové práce: *RNDr. Jiří Chudoba, PhD. Fyzikální ústav AV ČR*
E-mail vedoucího: Jiri.Chudoba@cern.ch

Abstrakt: *Byla prozkoumána metoda měření hmotnosti top kvarku na základě změřené délky doletu bottom hadronů a možnosti jejího využití v detektoru ATLAS. Byly porovnány různé popisy rozdělení těchto doletů a odhadnuty hlavní zdroje experimentální chyby. Pro účely analýzy byly vygenerovány případy dileptonového rozpadového kanálu s různými hmotnostmi top kvarku s použitím plných simulací v softwarovém prostředí Athena.*

Klíčová slova: *proton-protonové srážky, top kvark, ATLAS, Athena, měření hmotnosti*

Title: *The Measurement of Top Quark Mass in Proton–Proton Collisions in the ATLAS Detector*
Author: *Jan Pipek*
Departement: *Institute of Particle and Nuclear Physics*
Supervisor: *RNDr. Jiří Chudoba, PhD. Institute of Physics, AS CR*
Supervisor's e-mail address: Jiri.Chudoba@cern.ch

Abstract: *The decay length technique of top quark mass measurement and its possible use in the ATLAS detector were studied. The choice of parametrization describing the distribution of bottom hadron transverse decay length was investigated and main sources of uncertainties were identified. For this purpose 'dilepton' channel data samples with varying top quark masses were generated using full simulation in the Athena framework.*

Keywords: *proton-proton collisions, top quark, ATLAS, Athena, mass measurement*

In science one tries to tell people, in such a way as to be understood by everyone, something that no one ever knew before. But in poetry, it's the exact opposite.

Paul Dirac

Chapter 1

Introduction

The discovery of top quark was announced almost simultaneously at the beginning of March 1995 by both DØ[1] and CDF[2] collaborations at Tevatron. Since then its properties have drawn the attention of many scientists and many precise experimental and computational methods have been developed for the purpose of top quark studies. These facts are of no surprise considering the eminent position of top in the Standard model and theories beyond it.

All experimental data up to now come from Tevatron. However in the very near future LHC collider will begin operation and it will provide us with unprecedented possibilities of precise top quark measurements. Higher collision energy together with higher luminosity will ensure that we will observe more than 8 million $t\bar{t}$ pairs a year on each experiment.

One of the top quark properties which is studied most intensively is its mass – its value is important for putting constraints on several parameters of the Standard model (and its extensions), notably the mass of yet unobserved Higgs boson. Several methods exist that were successfully used to interpret data from both Tevatron detectors and made it possible to measure the top quark mass m_t with great precision.

Nevertheless there are methods that will highly benefit from the large statistics of the LHC as their utilizing at Tevatron is difficult due to the low number of recorded events. One of them is the *the decay length technique* which infers top quark mass from mean transverse decay length of bottom hadrons created during hadronization of bottom quarks, the daughter particles of decaying top quarks.

This work investigates the possible use of the decay length technique for precise measurements of top quark mass in the ATLAS detector.

> Things on a very small scale (like electrons) behave like nothing that you have any direct experience about. They do not behave like waves, they do not behave like particles, they do not behave like clouds, or billiard balls, or weights on springs, or like anything that you have ever seen.
>
> Richard P. Feynman

Chapter 2

Phenomenology and Motivation

2.1 The Role of Top Quark in the Standard Model

When top quark was discovered, it completed the third generation of elementary fermions[1] (elementary particles of the Standard model are listed in tables A.1 and A.2). Therefore its place in the Standard model is mainly that of an up-type quark, the $\mathrm{SU}(2)_L$ partner of the bottom quark.

Nevertheless due to its large mass top quark contributes significantly to many observables of the SM via loop corrections.

2.1.1 Higgs Boson Mass Constraints

Of these corrections the most important one constrains the possible values of the Higgs boson mass [3].

At tree level the mass of W can be written in terms of the SM parameters as

$$m_W^2 = \frac{\pi\alpha}{\sqrt{2}G_\mathrm{F}\sin^2\theta_W} \tag{2.1}$$

Higher level corrections modify this relation to

$$m_W^2 = \frac{\pi\alpha}{\sqrt{2}G_\mathrm{F}\sin^2\theta_W\,(1-\Delta r)} \tag{2.2}$$

[1] Although the tau neutrino was first directly observed in 2000.

In the next-to-leading order, the contributions of top quark and Higgs boson loops to the parameter Δr are given by

$$(\Delta r)_t \simeq -\frac{3G_F m_t^2}{8\sqrt{2}\pi^2}\frac{1}{\tan^2\theta_W} \tag{2.3}$$

$$(\Delta r)_H \simeq \frac{11G_F m_Z^2 \cos^2\theta_W}{24\sqrt{2}\pi^2}\ln\frac{m_H^2}{m_Z^2} \tag{2.4}$$

If the masses of top quark and W are known with enough precision the Higgs mass can be constrained. The interdependence of these three masses is illustrated in figure 2.1.

Figure 2.1: The interdependence of m_W, m_t and m_H

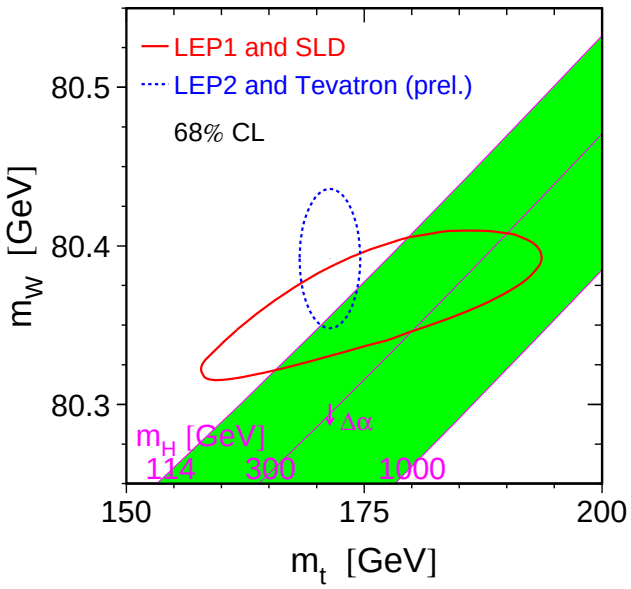

2.2 The Production of Top Quarks

Most top quarks are produced in pairs by strong interactions, via either quark-antiquark annihilation or gluon-gluon fusion (see figure 2.3), the latter being dominant at LHC with ~ 87 % of produced pairs (see figure 7.1 for more detail). This particularly stems from the fact that at LHC smaller part

of proton momentum has to be carried by initial state partons and lower x's prefer gluons to quarks. This is illustrated in figure 2.2 where parton distribution functions (multiplied by x^2 for better legibility) of individual partons are plotted (we used the CTEQ5M[4] set of functions in this figure). We set $Q = 175$ GeV to be of the order of top quark rest mass.

Figure 2.2: Parton distribution functions for $Q = 175$ GeV

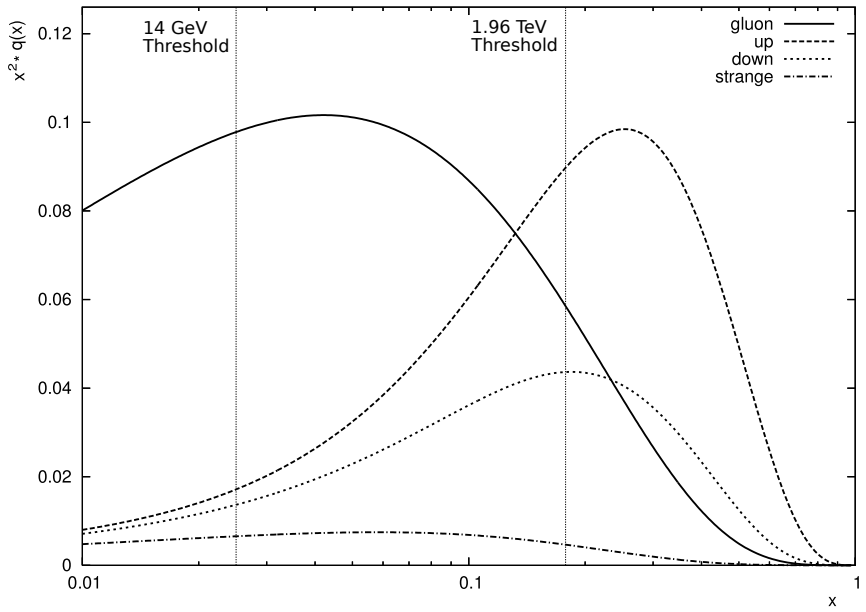

Single top-events (see figure 2.4 for their leading-order diagrams) produced by electroweak interaction suffer from lower cross-section and larger experimental background. They have not been directly observed at Tevatron yet and only cross-section constraints have been put.[2] Hopefully, LHC will bring more light to this area of top physics.

The theoretical NLO cross-sections of individual top production channels [6] [7] [8] for both Tevatron (1.96 TeV) and LHC (14 TeV) are summarized in table 2.1 (we list them without uncertainties because their definition differs from source to source).

2.3 Top Quark Decay

Within the SM, the top quark decays almost exclusively into a W boson and a bottom quark. If we restrict ourselves to the leading order and neglect

[2] The first evidence of single top quark was announced by DØ Collaboration in December 2006. [5]

Figure 2.3: Leading-order diagrams of $t\bar{t}$ production

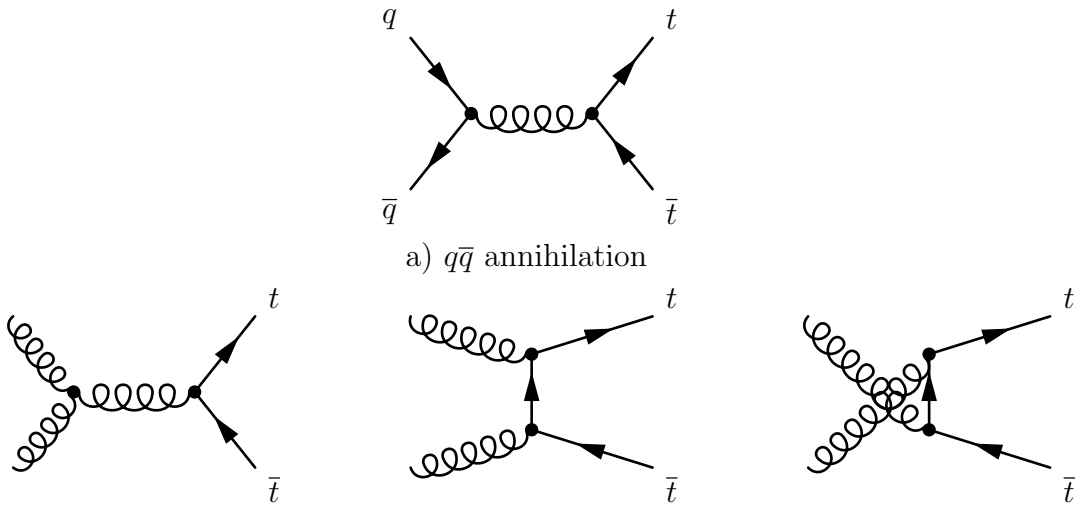

a) $q\bar{q}$ annihilation

b) gg fusion

Table 2.1: Top Production Cross Section (in pb)

Channel	σ_{Tevatron}	σ_{LHC}
$t\bar{t}$	6.97	833
s-channel	0.44	11
t-channel	0.99	247
Wt-channel	0.07	32

the mass of b quark, we can approximate the total decay width Γ_t of the top quark as [9]

$$\Gamma_t = \frac{G_{\text{F}} m_t^3}{8\pi\sqrt{2}} \left(1 - \frac{m_W^2}{m_t^2}\right)^2 \left(1 + 2\frac{m_W^2}{m_t^2}\right) \tag{2.5}$$

where G_{F} is the Fermi coupling constant. If we take the current experimental value of top quark mass we get the decay width of ~ 1.5 GeV which corresponds to the mean lifetime of $\sim 5 \cdot 10^{-25}$ s. This time is too short for the top quark to hadronize.

The final state of $t\bar{t}$ decay consists of two bottom quarks and the decay products of both child W bosons. S W boson decays in 2/3 cases to quark-antiquark pair, in remaining 1/3 with equal probabilities to a pair of a charged lepton and a neutrino of the same generation.

From the experimental point of view we distinguish these three useful channels (their branching ratios are illustrated in figure 2.5):

- **'All-jets' channel (44 %)** – Both W bosons decay hadronically, thus there are at least six jets present in the final state. This channel has the largest branching ratio, but it also has the largest background that disqualifies it from being the best channel for studying top properties.
- **'Lepton+jets' channel (30 %)** – One of the W's decays leptonically, the other hadronically. As tau leptons are hard to identify, they are often omitted from the studies. Because of that, we are left with 8/27 of $t\bar{t}$ events in this so-called 'golden channel'. There are four jets, one charged lepton and a significant missing transverse energy. Manageable background and large statistics result in this channel offering the most precise measurement of top quark mass using kinematic reconstruction.
- **'Dilepton' channel (5 %)** – Both W's decay leptonically and thus there are two jets, two leptons of opposite charge and a significant missing transverse energy carried away by two neutrinos. Again tau leptons are omitted. This channel has the clearest signature and lowest background – this was the main reason why it was selected for analysis in this work.

Figure 2.4: Leading order diagrams of single-t production

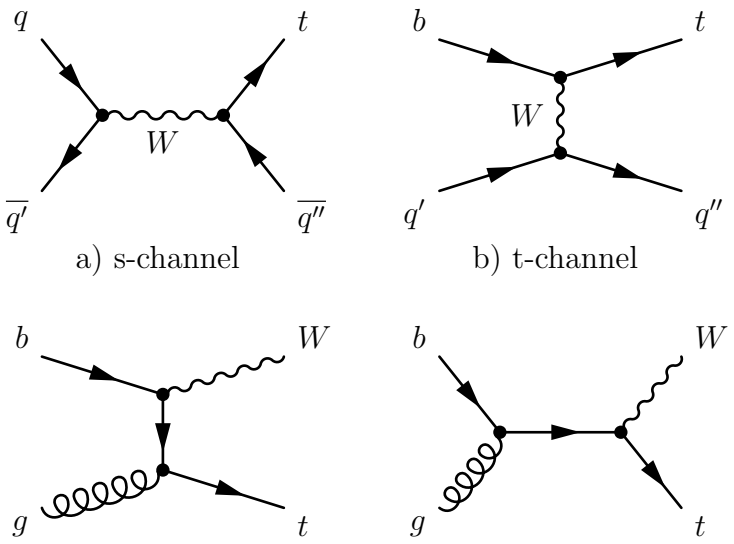

a) s-channel b) t-channel

c) Wt - associated production

Figure 2.5: Top quark decay channels [10]

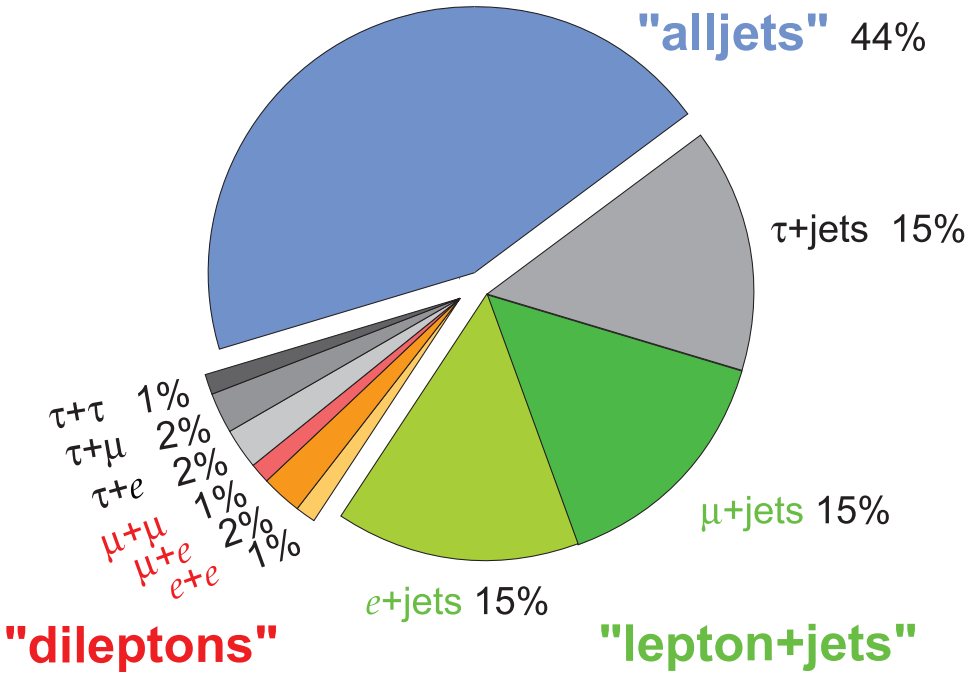

What we observe is not nature itself, but nature exposed to our method of questioning.

Werner Heisenberg

Chapter 3

Methods of the Top Quark Mass Measurement

3.1 Using the Kinematic Reconstruction of Events

Apart from the first indirect measurements of top quark mass using loop corrections at LEP and the single measurement using the decay length technique on CDF data [11], all contemporary measurements are done using kinematic reconstruction of $t\bar{t}$ events recorded at Tevatron experiments CDF and DØ.

The method of reconstruction differs from channel to channel – individual channels have different signatures, branching ratios, main background sources and naturally the completeness of kinematic information provided by the detector. In principle we need to select and combine proper three 'particles' (either three jets or a jet, a charged lepton and a neutrino) to calculate their invariant mass. Thus for full reconstruction four-momenta of six particles have to be found.

Neutrinos are not directly observable. In the case of the 'lepton+jets' channel we can substitute transverse momentum of the neutrino by missing transverse energy. The longitudinal momentum can be (with twofold ambiguity) obtained by fixing the invariant mass of lepton pair to m_W.

In the 'dilepton' channel more unknowns come into play and more constraints have to be put – the total transverse momentum of $t\bar{t}$ pair is assumed to be zero (see figure 7.3 for its simulated distribution), also the second lepton pair is required to have the invariant mass of m_W and finally top masses obtained from both parts of the event are considered to be equal – set as an input parameter for the reconstruction of event. Eventually the momenta of neutrinos can be obtained by solving a quartic equation [12]. To each

solution for different input top masses a weight is assigned (according to known distributions of several kinematic properties of $t\bar{t}$ events.). The top quark mass with the best sum of weights over all events becomes the result.

From the theoretical point of view the top quark mass should be easily obtained from the 'all-jets' channel or from the hadronic part of 'lepton+jets' events. However the correct assignment of jets to top quarks is not trivial and thus virtually all contemporary measurements in all channels stem from the usage of sophisticated techniques including the *template method* and the *matrix element weighting method*. Detailed descriptions of these methods and their applications on real data from Tevatron can be found in relevant papers [13, 14, 15, 16, 17].

All these channels can be investigated using similar techniques also in ATLAS. However the amount of events produced at LHC will allow us to concentrate on some rare but appealing samples with additional requirements put alongside the selection of one channel. Among others the final leptonic states with J/Ψ are of great expectation [18]. One can also select events that have top transverse momenta greater than a certain fixed value. An extensive summary of the ATLAS top quark measurement prospects is given in [19].

3.2 Using the Decay Length Technique

This method, first described in [20], promises a new way of top quark measurement, results of which should not be much correlated with those obtained using kinematic reconstructions. Even if it is not as precise as other methods[1] it will provide an important cross-check as it utilizes mainly data from the inner detector instead of the calorimeter system (main uncertainties of kinematic reconstruction are associated with jet energy scale).

3.2.1 Decay Kinematics

In the rest frame of the top quark, daughter particles (b quark and W boson) have momenta of the same magnitude:

$$p = \frac{c \cdot \sqrt{(m_t^2 - (m_W + m_b)^2)\,(m_t^2 - (m_W - m_b)^2)}}{2m_t} \approx 0.4\ m_t c \qquad (3.1)$$

[1] We believe it can significantly contribute to the reduction of world average measurement uncertainty.

Figure 3.1: The L_{xy} parameter[20]

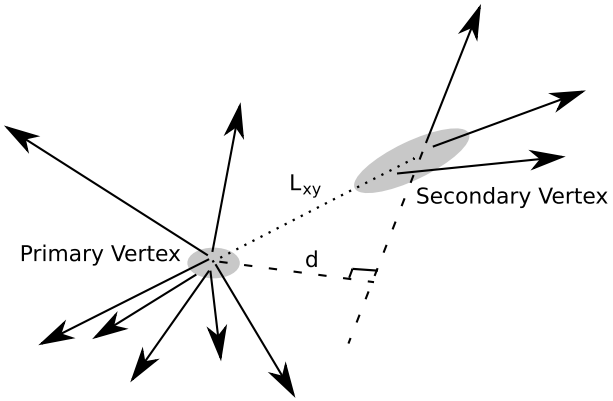

Due to this relation there is a strong correlation between top quark mass and transverse momenta of bottom hadrons (the contribution of top quark transverse momentum[2] is not negligible however it is small in comparison with the rest mass). Although observed values of b-jets p_T could be used, results would be directly dependent on the precision of hadron calorimeters. Instead of this we use the mean transverse decay length of bottom hadrons L_{xy} (illustrated in figure 3.1) as the primary source of information is the inner detector. Of course we need data from hadron calorimeters to identify the jets and measure their E_{T} for selection purposes, however individual values of L_{xy} are independent of calorimeter jet energy scale.

From the theoretical point of view, $\langle L_{xy} \rangle$ for a fixed bottom hadron p_{T} is equal to:

$$\langle L_{xy} \rangle = \frac{p_{\mathrm{T}}}{m_B} \cdot \tau_B \tag{3.2}$$

If we count with $\gamma \sim 10$, decay lengths of several millimetres can be expected. This is well within the detection of capabilities of the inner detector and of course b-tagging algorithms use the secondary vertex displacement as the main indication of a b-jet.

[2] See figure 7.5a) – mean transverse momentum of top quarks corresponds to a relativistic boost with $\gamma \sim 1.3$ in comparison with ~ 10 in the case of bottom quarks.

3.2.2 Top Quark Measurement

However the continuous bottom p_{T} spectrum and other factors rule out matching experimental data to a theoretical prediction. Therefore extensive use of Monte Carlo simulation is needed. We obtain distributions of L_{xy} for varying top quark masses and extract parameters that describe it. One finds $\langle L_{xy} \rangle$ itself as a natural choice, however other parameters can be used (e.g. exponential fit parameters). Selection of the most suitable parametrization is one of the main goals of this work.

Possible problems arise when tracks used for the secondary vertex reconstruction in b-tagging come from subsequent charmed hadron decay – some precision is lost in exchange for better tagging efficiency. However if we use same b-tagging algorithms for both simulation and real data, the L_{xy} distributions smeared due to this will remain consistent.

The first measurement using the decay length technique on CDF experimental data gives this value of top quark mass [11]:

$$m_t = 180.7^{+15.5}_{-13.4}\ (\text{stat.})\ \pm 8.6\ (\text{syst.})\ \text{GeV}/c^2 \tag{3.3}$$

The uncertainty of top quark measurement can at the ATLAS detector can reach the level of 1.5 GeV/c^2 after several years of running as expected by the authors of [20].

3.3 Current Experimental Value of Top Quark Mass

Multiple measurements from CDF and DØ using different techniques are combined to get the current top quark mass of [21]:

$$m_t = 171.4 \pm 1.2\ (\text{stat.})\ \pm 1.8\ (\text{syst.})\ \text{GeV}/c^2 \tag{3.4}$$

Measurements included in the combination are listed in figure 3.2.

Figure 3.2: Best independent measurements of the top quark mass [21]

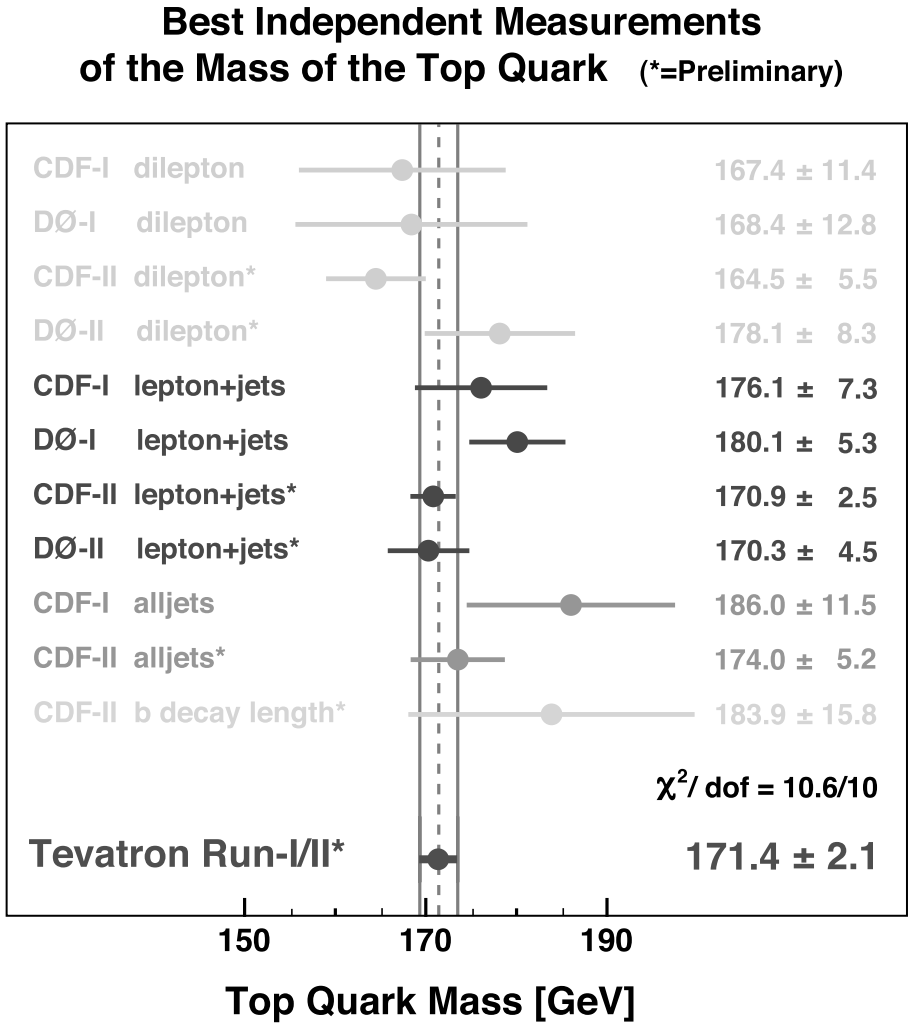

Any sufficiently advanced technology is indistinguishable from magic.

Arthur C. Clarke

Chapter 4

Experimental Setup

4.1 The Large Hadron Collider

The Large Hadron Collider [22] is a proton-proton (and ion-ion) collider being built in CERN. It is scheduled to begin operation in 2007 and it is going to become the world's highest energy collider in 2008. It is located in a tunnel which previously hosted the LEP (Large Electron-Positron Collider). The accelerator is designed to provide proton-proton interactions with total centre-of-mass energy of 14 TeV and to reach the luminosity $\mathcal{L} \sim 10^{34}$ s^{-1}cm^{-2}.

4.1.1 The Design of LHC

Because the LHC will accelerate two beams of identical particles two beam pipes are needed. Both pipes and magnets will be hosted in a single cryostat. The trajectory of particles is bent by 1232 superconducting NbTi dipole magnets cooled down to 1.9 K by superfluid helium, which create a magnetic field with the magnetic induction of 8.33 T. Additionally 392 main quadrupoles inserted in the straight sections of the ring are needed for the collimating purposes.

The protons with the kinetic energy of 50 MeV will be produced by linear accelerators, then accelerated consecutively by PS booster to 1.4 GeV, by PS (Proton Synchrotron) to 26 GeV and by SPS (Super Proton Synchrotron) up to 450 GeV before they will be injected into the beam pipes of the LHC itself.

At top luminosity, there will be 2808 bunches of protons orbiting in both beam pipes, each containing $\sim 10^{11}$ protons. At four interaction points, the beams will cross under an angle of 300 μrad with the frequency of

40.08 MHz. Because of the high luminosity there will be about 25 collisions in one bunch crossing, most of them being minimum-bias soft hadronic events.

Along the LHC ring, there are eight straight sections approximately 528 m long, where the RF accelerating cavities, the beam dump, cleaning devices and main experiments are placed. For the overall schema of LHC see figure 4.1.

Figure 4.1: The Large Hadron Collider

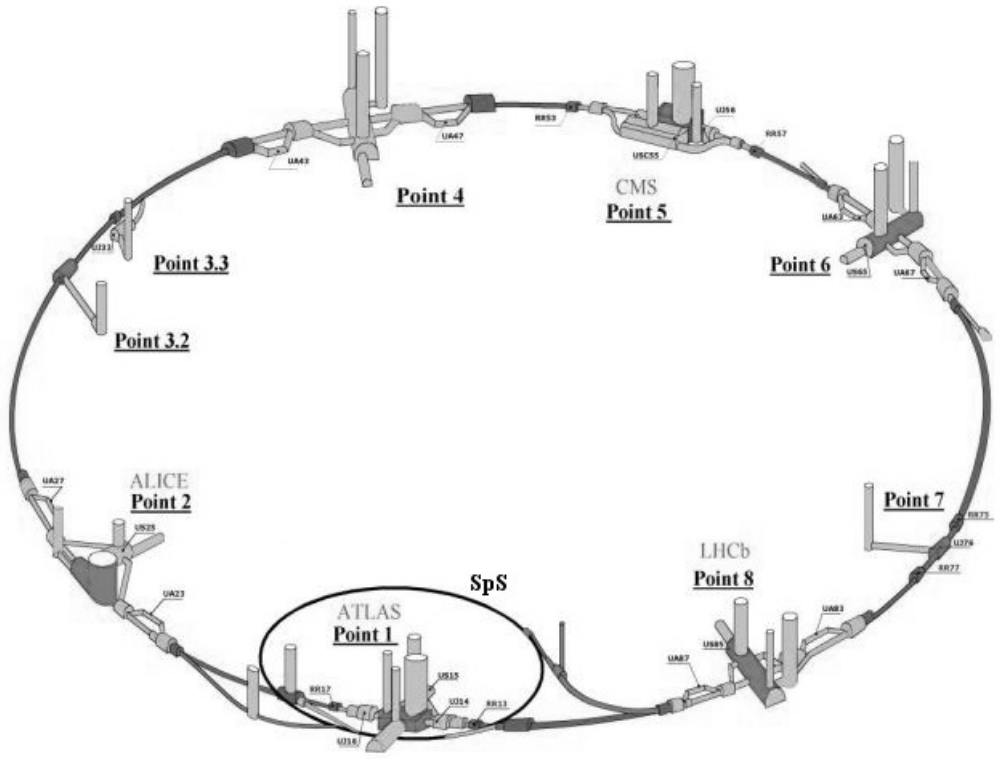

4.1.2 LHC Experiments

Two of the experiments - ATLAS (A Toroidal LHC ApparatuS) and CMS (Compact Muon Solenoid) are general-purpose experiments where the beams are focused to a small spot to achieve the maximum luminosity. The primary purpose of the low-luminosity LHCb (LHC-beauty) is the study of bottom physics.

Apart from protons the LHC is able to accelerate also the Pb ions, reaching the centre-of-mass energy of 5.5 TeV per nucleon pair. The ALICE experiment (A Large Ion Collider Experiment) is designed for the

study of ion-ion collisions. The peak luminosity of ion-ion collisions will be $\sim 10^{27}$ cm^{-2}s^{-1}.

4.1.3 The Goals of LHC

One of the main goals of the LHC is the search for the **Higgs boson**, or, more generally, the investigation of particle mass generation. Neither LEP nor Tevatron have directly observed the Higgs boson, however the experimental constraint for its mass has been put – at the confidence level of 95 %, it should be heavier than 114 GeV/c^2 [23]. The theoretical predictions of the Standard model exclude masses over ~ 1 TeV/c^2, so the whole possible range will be accessible at the LHC (with different dominant event signatures over this range).

However, the Standard model with Higgs does not satisfy the demand for a complete explanation of the spontaneous symmetry breaking and does not leave space for the unification of all known forces. Thus a more general theory is needed. Many have been proposed in the last decades, including **supersymmetry**, **technicolor** and the theories of compactified **extra dimensions**. Hopefully, non-trivial effects in favour of one of these theories will be observed. The experiments will be looking for new Z- or W-like particles and for the compositeness of fundamental fermions.

Although it was not designed for this purpose, the LHC will also produce huge amount of bottom quarks, thus there will be a wide window to **bottom physics** left open. The LHCb experiment is devoted solely to this topic.

Last but not least, the LHC will serve as a top factory. Due to a high production rate, almost all properties of the **top quark** will be measured with unprecedented precision, many of them even being measured for the first time.

4.2 The ATLAS Detector

ATLAS was designed as a general-purpose detector, capable of investigating a wide variety of physics signatures. The inner detector should be able to do reliable and precise vertexing and tracking of charged particles. The calorimeter system has to cover almost full space angle around the interaction point. The muon detector must provide a precise measurement of high-energy muons. The whole system should be as tight as possible for the

reconstruction of missing transverse energy. A complex magnetic system and a set of very efficient triggers is also needed.

To fulfil all these requirements, ATLAS is one of the world's largest experimental devices ever built. It has a barrel shape with a length of 44 m and a diameter of 22 m. The whole detector weighs roughly 7000 tons. For a general schematic view of ATLAS see figure 4.2. The whole experiment is fully described in [24], from which also the figures are taken.

Figure 4.2: The ATLAS Detector

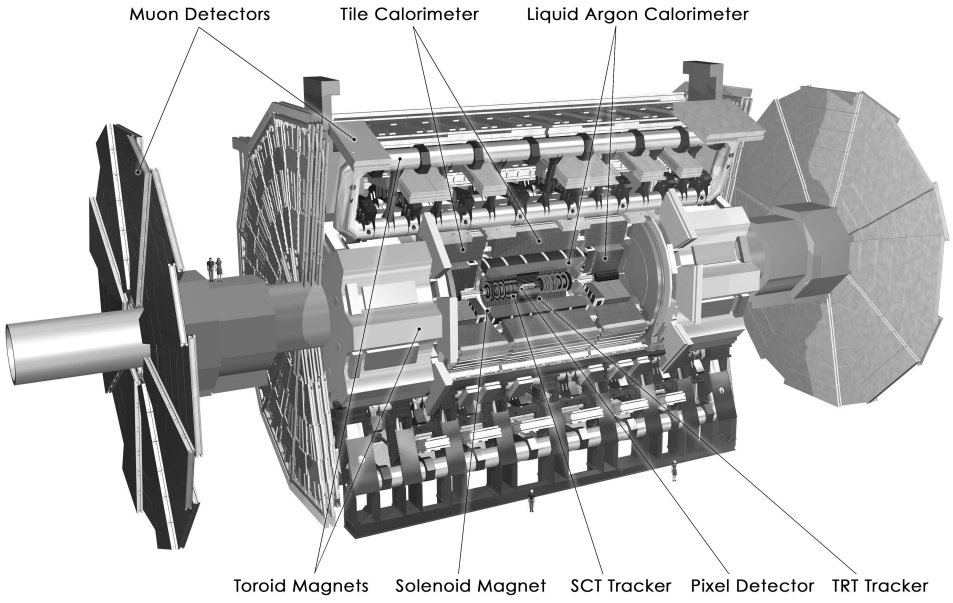

4.2.1 The Magnetic System

The magnetic system of ATLAS consists of four subsystems.

The super-conductive **Central Solenoid** (CS), placed in the LAr calorimeter cryostat and kept at the temperature of 4.5 K, provides the inner detector with a longitudinal magnetic field ranging from 2 T at the centre to 0.5 T at both ends. It is slightly shorter than the inner detector in order to reduce the amount of matter between the interaction point and the calorimeters.

Three air-core toroids are the source of magnetic field for the muon detector. Each of them consists of three flat coils assembled symmetrically around the beam axis. Individual coils of **Barrel Toroid** (BT) are placed in separate cryostats. Two **End-cap Toroids** (ECT) are placed in one

large cryostat each. The magnetic inductions of tangential fields in these toroids are 3.9 and 4.1 T respectively.

4.2.2 The Inner Detector

The Inner Detector [25] is situated in the cavity of the LAr calorimeter cryostat. It is 6.80 m long and its radius is 1.15 m. Its layout is shown in the figure 4.3. It is composed of three different detectors which cover the range of pseudorapidites $|\eta| < 2.5$ and provide enough points for tracking, vertexing and electron identification purposes.

Figure 4.3: The Inner Detector

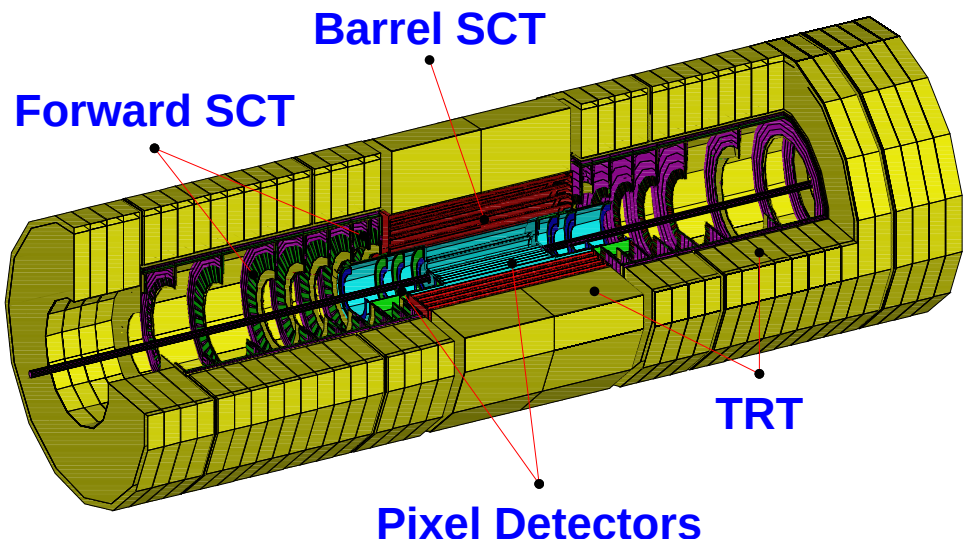

The **Pixel Detector** is placed closest to the beam line. There are three cylindrical layers at the distances of 50.5 mm, 88.5 mm and 122.5 mm from the beam line in the barrel part and additional three discs in both forward regions. There are 1744 silicon pixel sensors with a total number of 80 million pixels. The dimensions of one single pixel are 50×400 microns. The sensors overlap to make a hermetic coverage and so each particle should be detected in three pixel layers. The inner-most layer is exposed to enormous radiation and it is suppose to be replaced every few years.

The barrel part of the **Semiconductor Tracker** (SCT) consists of silicon microstrip detectors in four layers at radial distances from 30 to 52.5 cm. The end-caps are made of nine discs. The read-out channels have a resolution of 16 μm in $R\phi$ direction and 580 μm along the z-axis.

The **Transition Radiation Tracker** uses straw detectors 4 mm wide and up to 144 cm long. Its barrel part fills the space between 56 and 107 cm. The end-caps consist of 14 wheels covering the whole length of the inner detector. The straws are filled with a mixture of Xe, CO_2 and O_2 gases and equipped with a gold-plated tungsten wire. There are radiators between layers which produce X-rays, detected by xenon in the tubes for the electron identification. Each track should cross 36 straws on average.

The total uncertainties of track parameters, which are of principal interest for the vertexing purposes, can be approximately described as functions of p_{T} [24]:

$$\sigma(d_0) \approx 11 \oplus \frac{73}{p_{\mathrm{T}}\sqrt{\sin\theta}}\,(\mu\mathrm{m}) \tag{4.1}$$

$$\sigma(z_0) \approx 87 \oplus \frac{115}{p_{\mathrm{T}}\sqrt{\sin^3\theta}}\,(\mu\mathrm{m}) \tag{4.2}$$

$$\sigma(\phi) \approx 0.075 \oplus \frac{1.8}{p_{\mathrm{T}}\sqrt{\sin^3\theta}}\,(\mathrm{mrad}) \tag{4.3}$$

$$\sigma(\cot\theta) \approx 0.70 \times 10^{-3} \oplus \frac{2.0 \times 10^{-3}}{p_{\mathrm{T}}\sqrt{\sin^3\theta}} \tag{4.4}$$

$$\sigma\left(\frac{1}{p_{\mathrm{T}}}\right) \approx 0.36 \oplus \frac{13}{p_{\mathrm{T}}\sqrt{\sin\theta}}\left(\mathrm{TeV}^{-1}\right) \tag{4.5}$$

4.2.3 The Calorimeters

The purpose of the calorimeter system is to measure the energy carried by photons, electrons, taus and hadrons with sufficient precision and to shield the muon spectrometer from intensive radiation. The system is depicted in figure 4.4. Over a wide range of pseudorapidities, the particle showers stand before the total of 25 radiation and 11 interaction lengths.

Electromagnetic Calorimeter

Both the barrel part and the end-caps of the electromagnetic sampling calorimeter are composed of thin accordion-shaped layers of lead absorber and liquid argon active material. The shape ensures that the electron showers cross many layers of material and thus can be detected with great sensitivity. The calorimeter covers the pseudorapidities $|\eta| < 3.5$. In the central

Figure 4.4: The Calorimeters

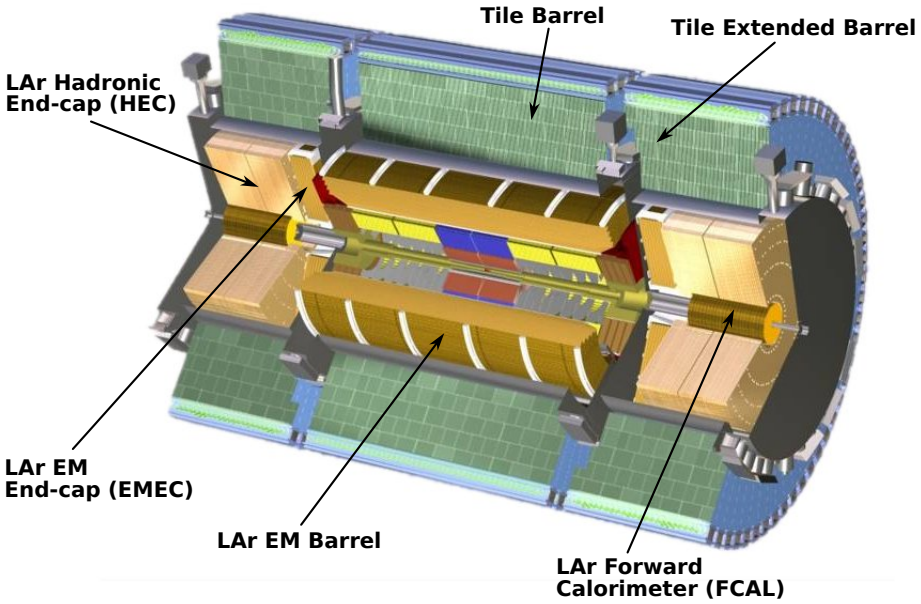

region, the main calorimeter is preceded by the presampler for the correction of energy loss. The granularity (in $\delta\eta \times \delta\phi$) is 0.003×0.1, 0.025×0.025 and 0.05×0.025 in three separate layers.

Hadronic Calorimeters

The range of pseudorapidities $|\eta| < 1.7$ is covered by the **Tile Calorimeter**, divided into central barrel and its two extensions. There are three radial layers - two of them segmented into 0.1×0.1 sections (in $\delta\eta \times \delta\phi$) and the last one into 0.2×0.1 sections. TileCal combines the steel absorber with plastic scintillators, connected by wavelength-shifting fibres to photomultipliers. The inner radius of TileCal is 2.28 m and the outer 4.23 m. The length of the central barrel is 5.64 m and both extended barrels are 2.91 m long.

The **LAr Hadron End-cap** shares one cryostat with LAr electromagnetic calorimeter end-cap and also with the LAr Forward Calorimeter. LAr was chosen because it is more resistive to high radiation in this region of pseudorapidities between 1.5 and 3.2. The absorber layers are made of copper.

LAr Forward Calorimeter (FCAL) detects electromagnetic showers as well as hadrons and it covers the pseudorapidity interval from $|\eta| = 3.2$ to $|\eta| = 4.9$. It is made of copper and tungsten with longitudinal tunnels

filled with liquid argon.

The energy resolution of the hadronic calorimeter can be expressed as follows:

$$\frac{\sigma\left(E\right)}{E} = \frac{A\%}{\sqrt{E}} \oplus B\% \tag{4.6}$$

The first term (sampling term) is given by the geometry and segmentation of the calorimeter, the second term comes from the imperfections in the material, the electronic noise and pile-up. The requirements for both the barrel and end-cap parts ($\frac{\sigma(E)}{E} = \frac{50\%}{\sqrt{E}} \oplus 3\%$) and also for the forward region ($\frac{\sigma(E)}{E} = \frac{100\%}{\sqrt{E}} \oplus 10\%$) are met.

4.2.4 The Muon Spectrometer

Being the outermost part, the complex muon spectrometer defines the dimensions of the ATLAS. The whole system is placed in a strong toroidal magnetic field provided by the Barrel Toroid, End-cap Toroids or a combination of both. The muons are subsequently measured in three chamber layers – Monitored Drift Tubes (MDTs) in the central region and Cathode Strip Chambers (CSCs) in the region of higher pseudorapidities and near the beam line – at different distances from the interaction point.

Additional measurements are provided by the muon trigger system composed of Resistive Plate Chambers (RPCs) in the central area and Thin Gap Chambers in the end caps.

The muon spectrometer covers the range of pseudorapidities $|\eta| < 2.7$ and provides precise identification and p_{T} measurement of muons. The reconstruction efficiency exceeds 90 % for muons with $p_{\mathrm{T}} > 6$ GeV/c and the relative uncertainty of p_{T} keeps under 2 % in the interval $6 < p_{\mathrm{T}} < 100$ GeV/c, slowly rising to 5 % for a 1 TeV-muon.

4.2.5 The Trigger System

At high-luminosity there will be $\sim 10^9$ events per second. Due to storage and data transfer limits, this rate has to be reduced to about 100 Hz. For this purpose, a three-level trigger system was designed. The overall schema of the trigger is presented in figure 4.5.

Figure 4.5: The Trigger System

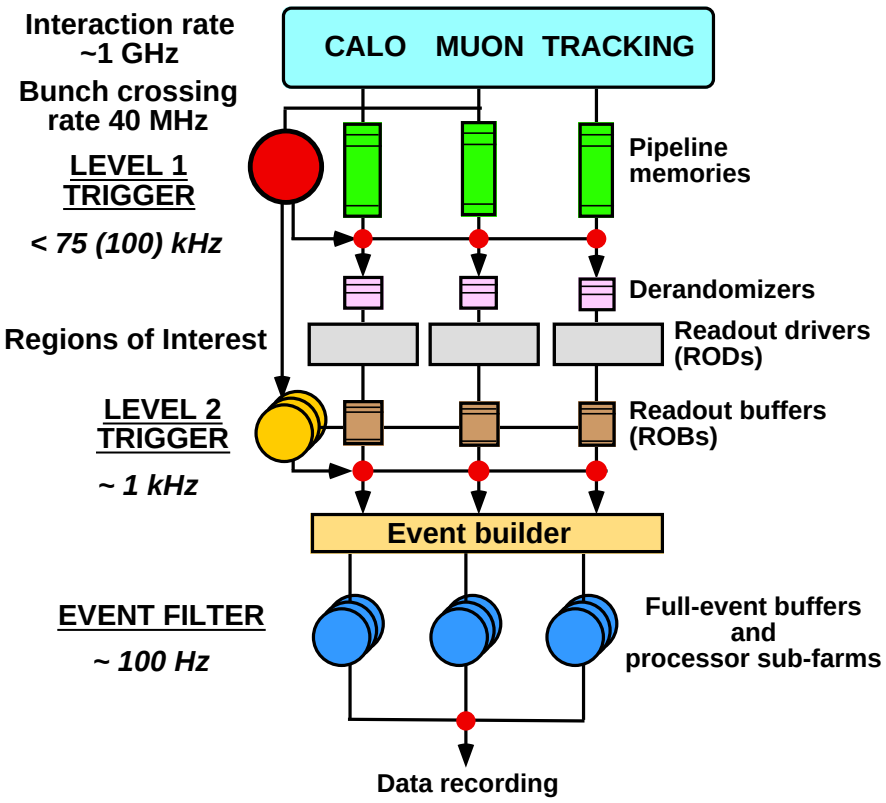

The **Level-1 Trigger** employs only data from the fast muon triggers (Thin Gap Chambers and Resistive Plate Chambers) and from calorimeters with a reduced granularity and decides before all data are collected by Read Out Drivers (RODs). Regions of interest are selected for more detailed analysis in higher-level triggers. The maximum output rate of this trigger is 100 kHz.

The **Level-2 Trigger** reconstructs the fraction of data coming from the regions of interest. Several physical signatures can be looked for. The rate is reduced to 1 kHz. Events which have passed this trigger are fully reconstructed by the Event Builder and then examined for the last time by the **Event Trigger**. Eventually the selected events are recorded.

Just because some of us can read and write and do a little math, that doesn't mean we deserve to conquer the universe.

Kurt Vonnegut Jr.

Chapter 5

Software Overview

5.1 The Athena Framework

Athena is an object-oriented framework used for ATLAS offline computing, based on the GAUDI architecture developed originally for the LHCb experiment. It uses C++ as its main programming language however it is possible to write one's own analysis completely in Python without much difficulty.[1] Athena provides controlling mechanisms for the interoperation among many independently-developed software packages and incorporates many utilities and common functionalities that can be reused in a wide range of concrete analyses.

The preferred method of data handling is using the **Transient Data Store** – a black-board system to which data are posted and read from instead of being passed directly between algorithms. It also provides access to data stored in external files and possibly other remote source. It is controlled via the **StoreGate** service. Several more services provide e.g. messaging or histogramming capabilities. The whole ROOT framework is also accessible from Athena.

Instead of writing standalone applications one has to implement user *algorithms*. From the programmer's point of view, algorithm is a class derived from the abstract `Algorithm` class. The run of algorithms is controlled by the Athena framework and thus explicit instantiation is not needed. One just needs to implement three pure virtual methods – `initialize()`, `execute()` and `finalize` which are called by the Athena job. Properties can be also declared in the class (using the `declareProperty()` method).

[1] This approach was also tested during our work but the algorithms developed in release 11 did not work in release 10 and thus this way abandoned. However it could be recommended for future use when backward compatibility is not needed.

The run of Athena is controlled by job options - little scripts written in Python that define which services should be loaded and which algorithms should be executed. It is also possible to set various properties of both algorithms and services and to specify the source of data to be processed. It is also possible to run algorithms interactively.

Atlas software is divided into small parts called packages that are developed continuously and are often available in several different versions. The CMT tool is used for automatic management of package dependencies and build process.

The Athena framework is documented in detail in [26] and [27], useful tutorials can be found in [28], [29] and [30].

5.2 The Full Simulation

The purpose of full simulation, a long and CPU-consuming process, controlled by Athena job options, is to simulate how the physics processes will be observed at ATLAS. The overall schema of the simulation chain is presented in figure 5.1. The job options used in the full simulation are listed in C.

Figure 5.1: The Schema of Full Simulation Chain [31]

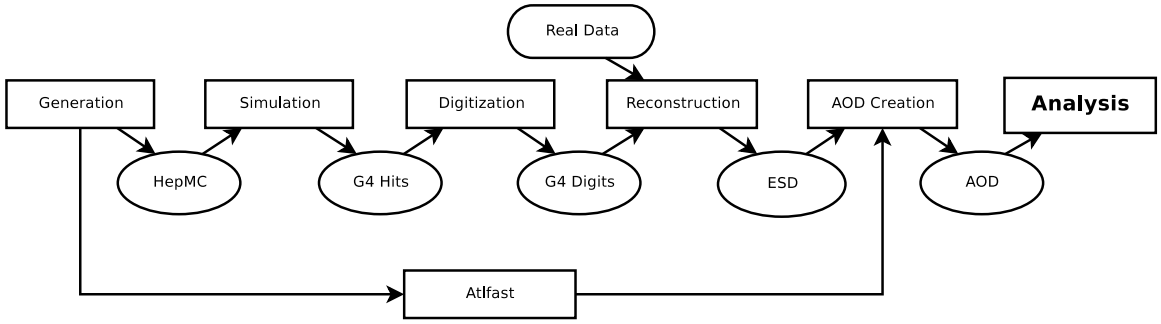

5.2.1 Generation

As the first stage of the full simulation chain, the physical event itself is generated by one of the Monte Carlo generators or their combination, including the hard process itself, initial and final-state radiation, parton fragmentation and the decays of particles in the final state of the event. In top-quark

physics several generators are used, each of them being suitable for different variety of studies [32].

Pythia [33] is a general-purpose Monte Carlo generator, that is used either on its own in simple analyses (like the mass measurement studies) or in combination with more precise matrix-element generators. Pythia itself calculates the matrix elements of top pair production in the leading order but it does not include information on top polarization (which is needed for the study of spin correlations).

TopRex has generally the same matrix-element generation capabilities as Pythia, however it includes the polarization information. **Alpgen** is powerful in producing additional partons but it does not smear the top quark mass with a Breit-Wigner distribution like other generators do. **MCAtNLO** is the only generator that calculates matrix elements in the next-to-leading order, while the main advantage of **AcerMC** is that it calculates matrix elements of the full $2 \rightarrow 6$ process. All four are only matrix element generators and thus a further development of event using Pythia (or **Herwig**) is needed.

In Athena, the output of Monte Carlo Generator is stored in HepMC objects that are later accessed in further full-simulation steps.

5.2.2 Simulation

For the simulation purposes GEANT4 is used. This tool simulates with enough precision the passage of particles through matter. The geometry of the detector and the materials used are described in full detail. The output of GEANT4 running is the energy deposition in active parts of the detector – the so-called 'hits'.

5.2.3 Digitization

In the digitization phase of full simulation, energy hits deposited in active parts of the detector are translated into the language of electronic signal to mimic the output of detector when real data are measured. Read-out effects like electronic noise are included.

The output of digitization is stored into **Raw Data Objects** files that contain the full description of the detector response. These files are however too large and they are not ready for physics analysis. However at this point real data obtained from the detector will enter the process.

5.2.4 Reconstruction

During the last stage the signal (a long series of bytes) is converted to physics quantities – tracks are reconstructed, the energy of jets is calculated from the energy deposition in calorimeters and particles are identified.

Files of three types can be created [34]:[2]

- **Event Summary Data** (ESD) contain all low-level reconstruction data like particle tracks and calorimeter clusters. One event should take about ~ 500 kB of disk space.
- **Analysis Object Data** (AOD) are suitable for most physics analyses. They contain reconstructed particles like electrons, muons, jets (with appended b-tagging information) etc. Apart from this truth information from the Monte Carlo generator is included. A backward link to ESD is possible if additional information is needed. AOD can be generated either from ESD or independently. The total size of event is about 100 kB. The list of object containers stored in AOD from full simulation with default settings is presented in D.
- **Tags** – these files contain only the basic characteristics of events in ~ 1 kB per event and they are intended for fast event selection.

[2] In previous releases data stored in ROOT TTrees in CBNT (ComBined NTuple) files were also used but their usage is now discouraged.

Finagle's First Law: If an experiment works, something has gone wrong.

Murphy's Laws of Research

Chapter 6

Data Selection

6.1 Data Samples

As we were interested primarily in individual b jets and their corresponding secondary vertices and because the method of top mass reconstruction is independent of other particles coming from the interaction, we needed a decay channel with a clear signature and a negligible background. Among the decay channels of top quark pairs, the 'dilepton' channel satisfies both these criteria.

Its event signature is very clear (two b jets, two opposite charge leptons with high p_T and a significant missing E_T) and the background is manageable (this is discussed later in this section). The fraction of events is small ($\sim 5\%$) compared to other two main investigated channels. This is a source of considerable statistical uncertainties when analyzing the Tevatron data (the authors of [20] employed the 'lepton plus jets' channel instead), but the large number of top quark pairs produced at LHC allows us to stick to this pure channel in the future – one year of running at low luminosity (with an integrated luminosity of ~ 10 fb^{-1}) will provide us with as much as 400,000 'dilepton' events.

6.1.1 Events Generated in Pythia

Because running the full simulation chain is very CPU-consuming (it takes about 20 minutes to simulate one event on a typical present-day processor), we studied the parton-level properties and several sources of systematic uncertainties separately using the events generated by Monte Carlo generator Pythia 6.319 (event generation is about five orders of magnitude faster than full simulation). Another advantage of this approach is that it is possible

to run Pythia independent of Athena on a desktop machine without much configuration effort (for that matter, it is well integrated into ROOT).

Pythia was set up to produce 'dilepton' events. For such purpose, we restricted the generation of events to $t\bar{t}$ pairs only and switched all hadronic decay channels of W bosons off.

We generated 200,000 events for each of eleven different hypothetical masses of top quark ranging from 150 to 200 GeV/c^2. Additionally we generated similar samples for examining various systematic uncertainties – just for the top quark mass of 175 GeV/c^2. In Appendix B we list Pythia parameters that were used to obtain them.

6.1.2 Events from the Full Simulation

In order to explore the area of different physics channels and because of our requirements we used data samples coming from various sources and reconstructed using different versions of ATLAS software. In all cases (due to storage capacity constraints and availability) the AOD (Analysis Object Data) files were used. These data files provided us with enough abstraction (the analysis begins with reconstructed particle objects instead of individual tracks or calorimeter hits), although it brought about several difficulties. Many particles were reconstructed twice (or more times), once as electrons and once as jets. What might be even more painful for our analysis, the collection of truth particles stored in AODs is very limited and it lacks data about vertices. Because of these limitations, we had to loosen the event selection criteria and to gather all vertexing information from b-tagging output.

The use of ATLFAST was rejected in this work because of the simple probabilistic way it approaches the b-tagging problem and because vertex info cannot be accessed as easily as in full-simulation data. Nevertheless fast simulations could be used instead of Pythia-generated events for the estimation of systematic errors with better precision.

Rome Production Samples

These data come from the production for the Rome Atlas Workshop in 2005. They were generated using various Monte Carlo generators (TopRex with Pythia for the top pair events, MCAtNLO in combination with Jimmy for

the main part of the background and AcerMC for 4321 Zj sample). The simulation was done in Atlas software release 10 (10.0.1 if known) and therefore analysis was also compiled against this version (specifically 10.0.6). Most of the samples were downloaded from the website of Theoretical Physics Group of BNL [35] via HTTP although they're also available at Castor and can be obtained over Grid too.

Sample 4522 stands out for two reasons: It is of principal interest for us, because it is the only Rome sample containing (just) signal events. Secondarily, it is not generally listed among the other samples and is available only at Castor (`/castor/cern.ch/user/r/resende/dilep`). It was simulated using Atlas Software release 10.0.4. Here is the list of samples:

$t\bar{t}$ samples: 4522 (signal), 4520, 4521 (background).

Other background samples: 4160, 4161, 4162, 4163, 4164, 4165, 4166, 4134, 4135, 4136, 4137, 4139, 4144, 4130, 4131, 4132, 4133, 4121, 4122, 4123, 4321.

CSC 11 Data Samples

These data samples come from Computing System Commissioning production. They include Drell-Yan samples (5110, 5112, 5191), found by [36] to be important source of background, and 5200 – the all-inclusive sample of $t\bar{t}$ generated by a combination of MCAtNLO and Jimmy generators. These data were obtained from both BNL and from the storage elements of Golias farm using Grid tools.[1]

Simulated Events with Different Top Masses

Because there are no publicly available data samples with varying top quark masses, we had to generate our own data. We created five data samples for the hypothetical top masses of 165, 170, 175, 180 and 185 GeV/c^2 using Atlas software release 11.0.4. The process of simulation is described in section 5.2. As in the case of events for parton-level studies, we have restricted Pythia to generate only 'dilepton' events. We also generated a sample with $m_t = 175$ GeV/c^2 without final-state radiation as this source of uncertainty seemed most dangerous after studies on Pythia-only events. We include our job options files in section C.

[1] The list of available datasets can be obtained from the Panda Monitor webpage, http://gridui01.usatlas.bnl.gov:25880/server/pandamon/query/.

Because the full simulations are very CPU-consuming, we got only about 6000 events per sample after a month of running on ~ 20 processors of the Golias computing farm.

6.2 Selection Criteria

For the analysis of full-simulation samples, we accepted the *de facto* standard selection cuts proposed by [19] (with a tiny change in the lepton p_{T} requirements). We investigated (to some extent) their efficiency and ability of background suppressing. Further we studied how the choice of particular cut on jet E_{T} affects the mean transverse decay length of involved bottom hadrons.

No restrictions were put on the events generated in Pythia, because the correspondence between partons or hadrons and jets is not trivial and because the events are treated differently. The shift of the mean transverse decay length resulting from this is not really important because the goal of our Pythia studies was not to make a prediction of absolute $\langle L_{xy} \rangle$ that could be tested against data from full simulation.

6.2.1 The Selection Method

We examined the contents of electron, muon and jet containers as well as the missing E_{T} information in the AODs.

Leptons

We required that there are two isolated leptons of opposite charge exceeding the p_{T} limit of 25 GeV/c, one of them further having at least 30 GeV/c. The isolation is defined as absence of reconstructed jets nearer than 0.45 in the $\eta\phi$-plane. Leptons with $|\eta| > 2.5$ were also excluded.

Electrons were taken from the `ElectronCollection` container. We required that their `isEM` bit array was empty (that means they were reconstructed using full tracking information from the inner detector and also from the calorimeters).

Muons were taken from the `MuonCollection` container in Rome samples and from the `MuidMuonCollection` container in the samples from the release 11.

Individual leptons that did not pass any of the cuts were ignored – they did not induce the rejection of event. However (as described later) lepton cuts were not applied when studying the pure sample in order to get higher statistics.

Jets

We took jets from the `BJetCollection` container where also the b-tagging information is stored. Our criteria required that there were exactly two jets with $E_{\mathrm{T}} > 25\mathrm{GeV}$ and $|\eta| < 2.5$. The b-tagging likelihood (combined from more b-tagging tools) of both jets had to be over 0.5.

After an event was accepted, for further analysis we used only those jets that had `SecVtxBU` tagging info attached[2] and whose combined b-tagging likelihood exceeded 0.9 in order to reduce the background from wrongly reconstructed jet or mistagged light jets (there is a strong tail associated with them).

Missing Transversal Energy

We required that the missing transverse energy taken from `MET_Final` object exceeded 40 GeV.

6.2.2 Selection Efficiency

We collected a variety of background channels and tested the rejection ability of our selection cuts on them. In tables 6.1 and 6.2 we list the numbers of events coming from individual channels that were accepted as well as estimated number of events passing our cuts after an integral luminosity of 10 fb^{-1}.

Background Rejection

We investigated several diboson samples and three $Z \to \ell\ell$ + jets samples from Rome production. We identified the most significant source of background to be the $Z \to \mu^+\mu^- + j$ sample and roughly estimated the signal-over-background ratio to be about 5 to 1.

[2] Because one false event with the L_{xy} of more than 1 m was found in the sample and this single entry significantly shifted the mean value, we additionally added a condition $L_{xy} < 500$ mm – this corresponds to the mean decay length of a bottom hadron with $p_{\mathrm{T}} \sim 5$ TeV/c.

Table 6.1: The efficiency of selection cuts on Rome samples.

Sample	Process	σ [pb]	Events passed (total)	Efficiency [%]	Events ($10\ \text{fb}^{-1}$)
4121	$Z \to e^+e^- + j$	4730×0.10 [37]	0 (83736)	~ 0	< 100
4122	$Z \to \mu^+\mu^- + j$	4730×0.11 [37]	8 (98879)	0.01	~ 400
4123	$Z \to \nu\bar{\nu} + j$	6140×0.12 [37]	0 (103725)	~ 0	< 100
4130	$WW \to \ell\ell\nu\nu$		0 (7943)	$\lesssim 0.02$	
4131	$WW \to \ell\tau\nu\nu_\tau$		0 (2530)	$\lesssim 0.05$	
4132	$WW \to \ell\nu j$		1 (22276)	$\lesssim 0.01$	
4133	$WW \to \tau\nu_\tau j$		0 (11062)	$\lesssim 0.01$	
—	All WW	127.5	1 (43811)	< 0.01	$\lesssim 30$
4134	$ZW^- \to \ell\ell\ell\nu$		3 (6230)	~ 0.05	
4135	$ZW^+ \to \ell\ell\ell\nu$		3 (26829)	~ 0.01	
4136	$ZW^+ \to \tau\tau\ell\nu$		0 (13294)	~ 0	
4137	$ZW^+ \to \ell\ell\tau\nu_\tau$		4 (14365)	~ 0.03	
4139	$ZW^- \to \ell\ell\tau\nu_\tau$		0 (97)	$\lesssim 1$	
4144	$ZW^- \to \tau\tau\tau\nu_\tau$		0 (3659)	~ 0	
—	All ZW	57.7 [38]	10 (64474)	~ 0.02	~ 90
4160	$ZZ \to \ell\ell\ell\ell$		0 (731)	$\lesssim 0.1$	
4161	$ZZ \to \ell\ell\tau\tau$		2 (2289)	~ 0.1	
4162	$ZZ \to \ell\ell j(j)$		5 (7839)	~ 0.1	
4163	$ZZ \to \tau\tau j(j)$		1 (6087)	~ 0.01	
4164	$ZZ \to \ell\ell\nu\bar{\nu}$		7 (11213)	~ 0.05	
4165	$ZZ \to \tau\tau\nu\nu$		0 (9218)	$\lesssim 0.01$	
—	All ZZ	16.8 [38]	15 (37377)	~ 0.04	~ 80
4321	$Zbb(4\ell)$	49×0.013 [39]	265 (48223)	0.5	~ 40
4520-1	$t\bar{t} \to b\bar{b}jj\ell\nu$	247	24 (183108)	0.01	320
4522	$t\bar{t} \to b\bar{b}\ell\ell\nu\bar{\nu}$	41	1177 (96862)	1.2	4980

Table 6.2: The efficiency of selection cuts on CSC11 and custom samples.

Sample	Process	σ [pb]	Events passed (total)	Efficiency [%]	Events (10 fb^{-1})
5110	$Z \to \mu\mu$	9217×0.019 [40]	0 (9999)	$\lesssim 0.01$	$\lesssim 200$
5112	$Z \to ee$	1650×0.479 [40]	0 (9999)	$\lesssim 0.01$	$\lesssim 800$
5191	$Z \to \mu\mu$	1650×0.094 [40]	0 (12999)	$\lesssim 0.01$	$\lesssim 120$
5200	$t\bar{t}$	833	123 (107999)	0.12	9500
165 GeV/c^2		~ 41	72 (6675)	1.1	4400
170 GeV/c^2		~ 41	76 (6714)	1.2	4600
175 GeV/c^2		41	74 (6840)	1.1	4400
180 GeV/c^2		~ 41	94 (6350)	1.5	6070
185 GeV/c^2		~ 41	103 (6811)	1.5	6200
175 GeV/c^2 (no FSR)		41	82 (5599)	1.5	6000

Cuts were also applied on three Drell-Yan samples from the CSC11 production – not a single event out of 33,000 passed passed the cuts, nevertheless a larger statistics would be needed to justify the omitting of this sample from analyses. [3]

Our limited statistics does not allow us to make a quantitative estimation of the uncertainty connected with the background, although the only channel with enough data (4321) is discussed in section 8.5.6.

Non-signal $t\bar{t}$ Channels

It should be noted here, that although we did not intend to include 'lepton+jets' and 'all-jets' channels in our studies, they differ from our signal channel only in the leptonic parts of events and therefore should give similar results.

We have shown that the impurity of 'lepton+jets' in the signal will be about 10 % and thus can not be neglected. On the other side, the rejection of 'all jets' events should be much stronger and the contribution of this channel should be minimal. Neither assumption could be tested as there were no 'all-jets' data available and the sample of 'lepton+jets' contains only 24 events after cuts are applied.

[3] One constraint, not present at the time of analysis, should help us eliminate background from leptonically decaying Z bosons: Events with the invariant mass of leptons within a narrow range around m_Z can be excluded from analysis without a significant reduction of signal events [36].

Table 6.3: Number of accepted events after the loosening of selection criteria

Sample	Accepted events		Total events
	before loosening	after loosening	
4522	1177	7790	96862
165 GeV/c^2	72	484	6675
170 GeV/c^2	76	473	6714
175 GeV/c^2	74	513	6840
180 GeV/c^2	94	491	6350
185 GeV/c^2	103	516	6811
175 GeV/c^2 (no FSR)	82	531	5599

Signal Efficiency

If we compare all signal samples we get efficiencies ranging from 1.1 to 1.5 % (plus the number of events from the all-inclusive 5200 sample comparable to 'dilepton' efficiency of 2%). We account that to statistical fluctuations and possibly to different settings of the reconstruction environment (our results in chapter 8 indicate that the latter effect can be surprisingly strong).

6.2.3 Criteria Loosening

Although ~ 1 % efficiency may be suitable for the amount of data collected by ATLAS after several fb^{-1} of integral luminosity, our small samples would become ruined by statistical error if we applied our strict cuts on them – we would be left with about one hundred transverse bottom decay lengths to analyse.

Because of that we chose a seemingly dangerous thing to do – to completely ignore the leptonic selection criteria when treating the pure signal samples. Of course we do not suggest to ignore them when studying real data. We just believe that $\langle L_{xy} \rangle$ (or any fit parameter which mimics it) taken from signal events does not change significantly if we forget the leptonic part of event.

Profile histograms in figure 6.1 show the dependence of $\langle L_{xy} \rangle$ on transverse momenta of bottom quarks and leptons and on the missing E_{T} taken from Pythia events with three different top quark masses. The first dependence is obvious (see equation 3.2), the other two are worth some discussion.

The histogram of lepton transverse momentum is plotted in figure 7.5.

A significant fraction of leptons has p_{T} below the selection cut of 25 GeV/c. Therefore we should be aware of them. Figure 6.1c) shows that leptons with low p_T slightly prefer bottom hadrons with higher L_{xy}. This is not surprising because of the correlation between the p_T of leptons and their source W's and the wide opening angle between the W bosons and the corresponding bottom quarks. Nevertheless the dependence is not strong and only a slight shift of $\langle L_{xy} \rangle$ should be expected. It should be possible to parametrize this shift using a linear function (however then there would be no need of this parametrization).

As missing transverse energy is a result of two (or more) neutrinos whose directions and momenta are almost uncorrelated and because two vertices are counted in each event, there is no dependence of L_{xy} apart from statistical fluctuations.[4] The effect of ignoring the missing transverse energy cut (40 GeV) is further suppressed by the fact that only a tiny fraction of events has missing E_{T} below this level (see figure 7.4).

After the selection criteria were loosened, we got about 5 or 6 times larger statistics (see table 6.3) which was just enough to make a linear fit of the dependence of $\langle L_{xy} \rangle$ on top quark mass with a relative uncertainty of the linear parameter being about 50%.

[4] However this holds only for the range of low missing E_{T}'s. On the contrary events with high missing E_{T} (i.e. $\gtrsim$ 120 GeV) need to contain at least one top quark with high transverse momentum and so the probability of a severely displaced vertex is larger.

Figure 6.1: Dependence of $\langle L_{xy} \rangle$ on p_{T} of different particles

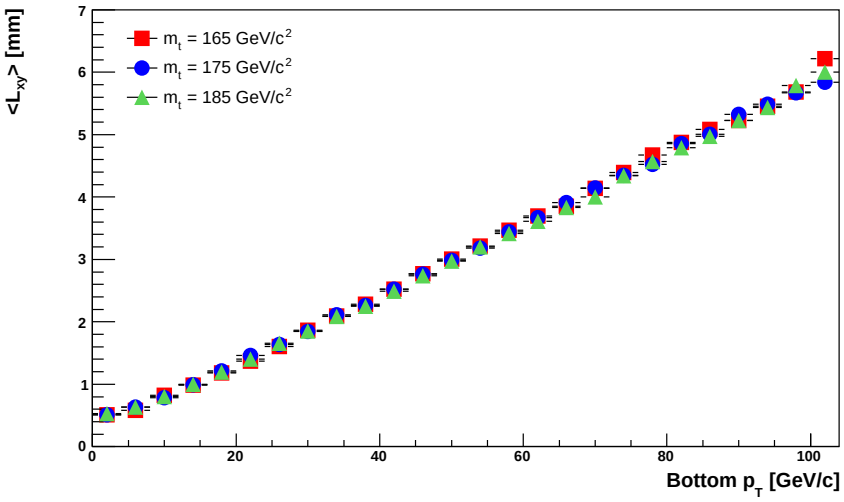

a) Bottom quarks

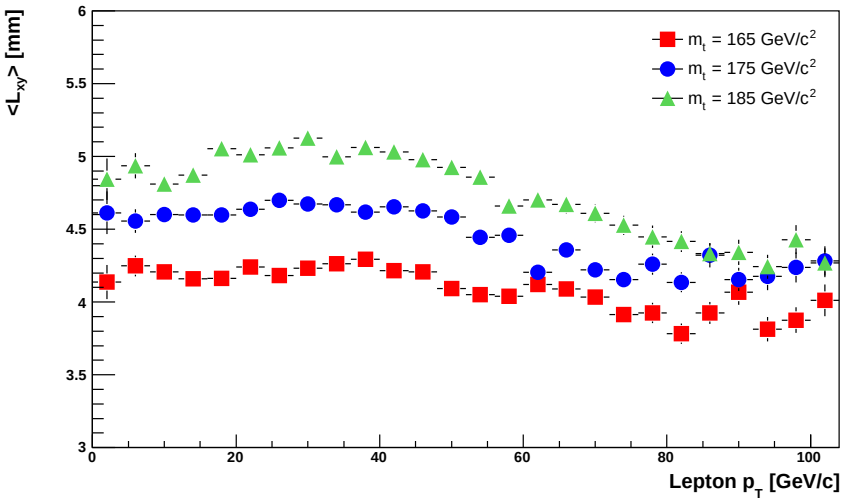

b) Leptons

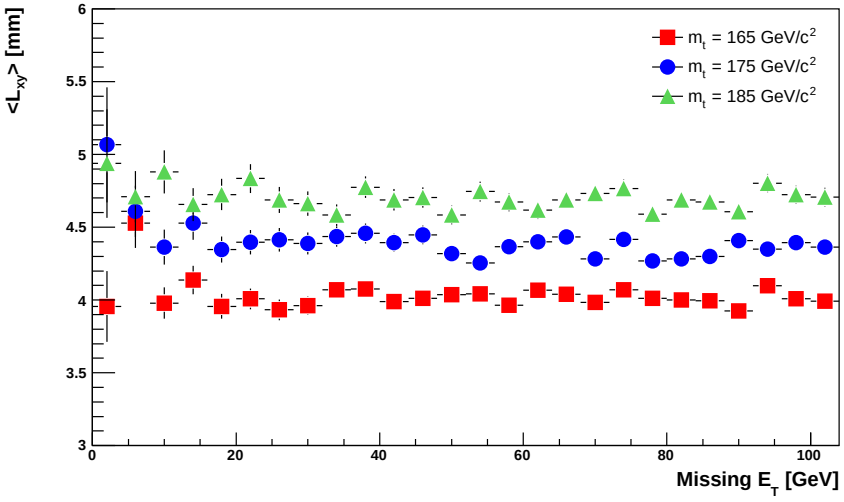

c) Missing transverse energy

Truth in science can be defined as the working hypothesis best suited to open the way to the next better one.

Konrad Lorenz

Chapter 7

Kinematic Properties of the 'Dilepton' Channel

In this chapter we briefly investigate the kinematic properties of 'dilepton' $t\bar{t}$ events. All data were extracted from the Pythia samples. We compare histograms of kinematic properties for three different masses of top quark (150, 175 and 200 GeV/c^2). Several properties are plotted over the whole range of masses. Apart from the selection of 'dilepton' channel and the setting of m_t, standard parameters of the generator remained intact.

7.1 The Production of Top Quark Pairs

Roughly 86 % of top quark pairs were produced via gluon fusion. However, the fraction of $q\overline{q}$ annihilation events slightly increases with the top quark mass (See figure 7.1).

Top quark pairs are produced near threshold, leaving $\sim$ 150 GeV for kinetic energy. This is illustrated in figure 7.2. The mean invariant mass naturally rises with the top mass (as seen on the second plot) and the peak slightly broadens.

Due to initial-state radiation (its effect is described in section 8.5.4.) the $t\bar{t}$ pairs often have non-zero transverse momentum. Its distribution is plotted in figure 7.3.

7.2 Transverse Momentum

We present the p_{T} spectra of top quarks and bottom quarks on the parton level, of the charged leptons (electrons and muons are not distinguished)

Figure 7.1: $q\bar{q}$ annihilation fraction

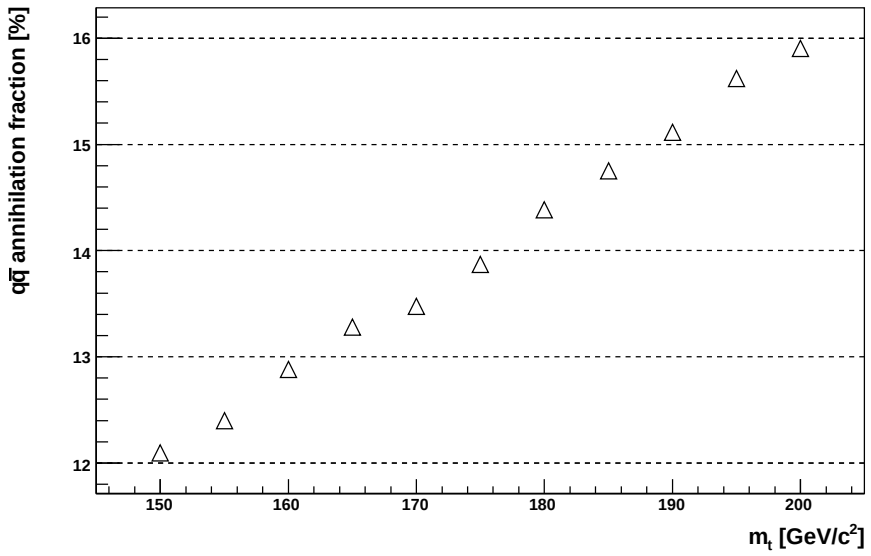

and of the bottom hadrons, whose decay vertices are taken for the analysis. See figure 7.5.

7.3 Pseudorapidity

We created histograms of pseudorapidity for four different types of particles (see figure 7.6). Not surprisingly, the distributions are symmetrical with respect to 0. All studied particles indeed do prefer directions perpendicular to beam axis – with the exception of top quarks which have maxima around $|\eta| \simeq 1.2$ (These maxima slightly lose their significance with growing m_t). It is apparent, that our requirement $|\eta| < 2.5$ does not reduce the statistics significantly.

Figure 7.2: Invariant mass of $t\bar{t}$ pairs – histograms and plot of $E_{\mathrm{CMS}}(t\bar{t})$ dependence on top quark mass. In histograms logarithmical scale was chosen.

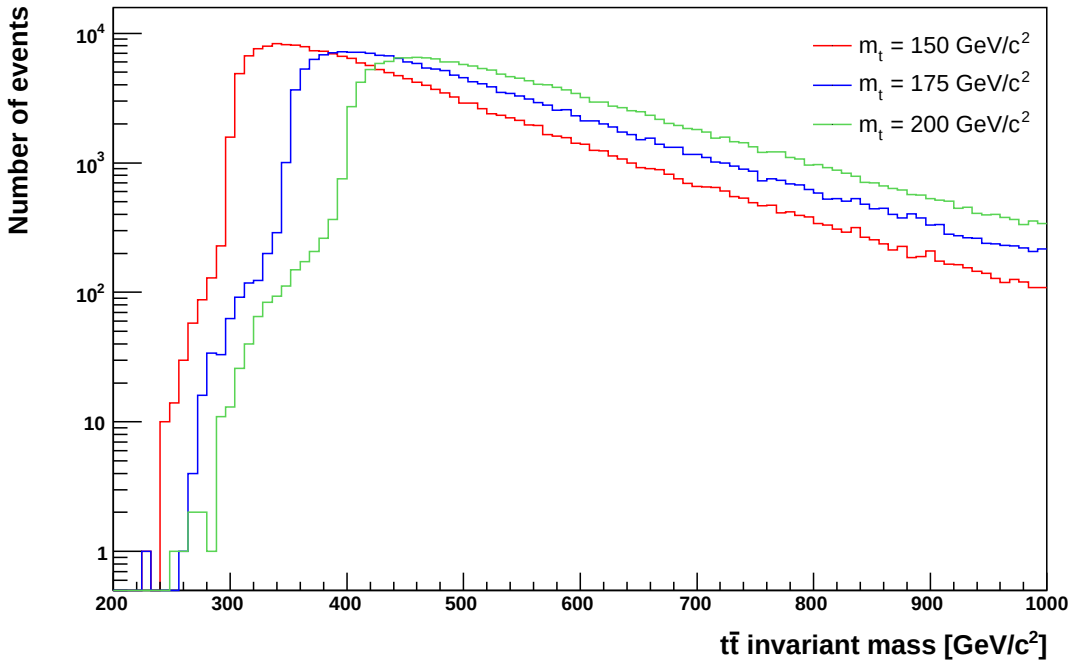

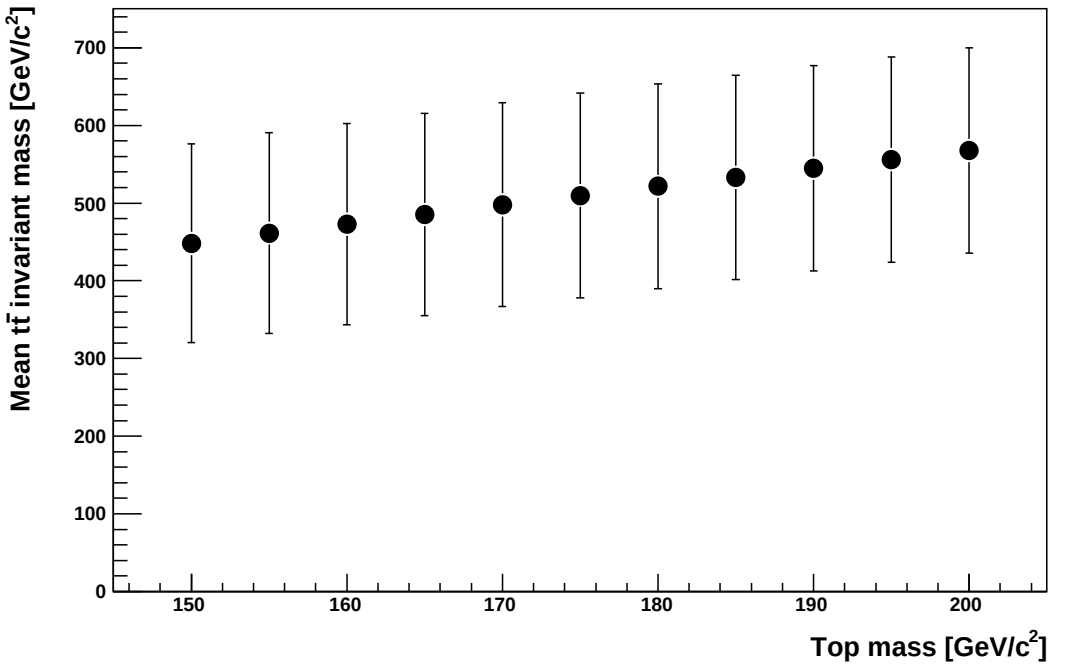

Figure 7.3: $t\bar{t}$ transverse momentum

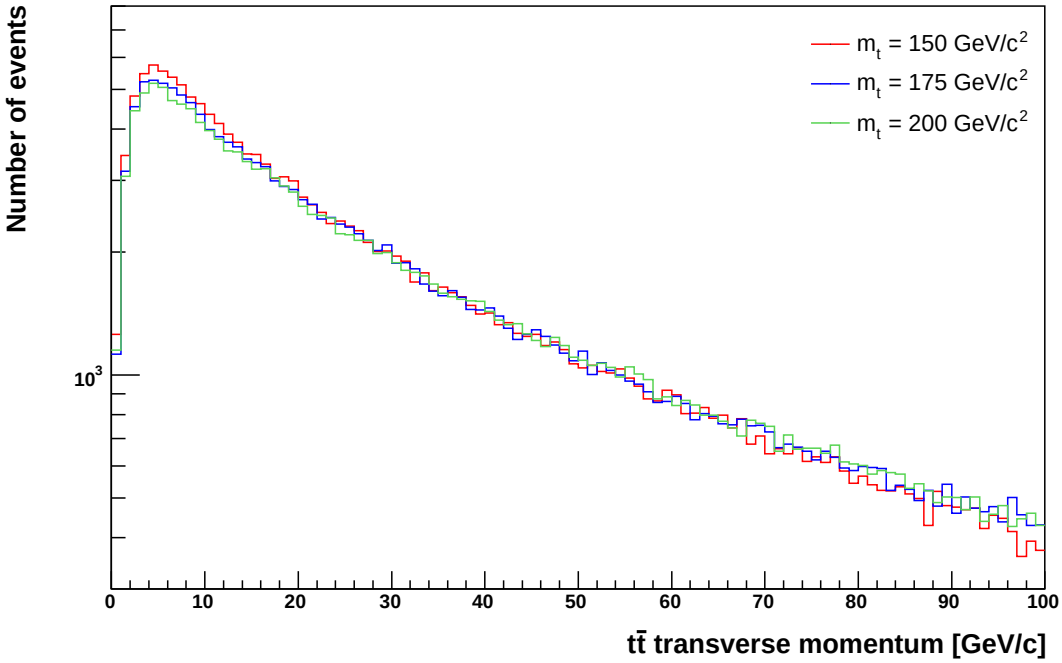

Figure 7.4: Missing transverse energy in dilepton events

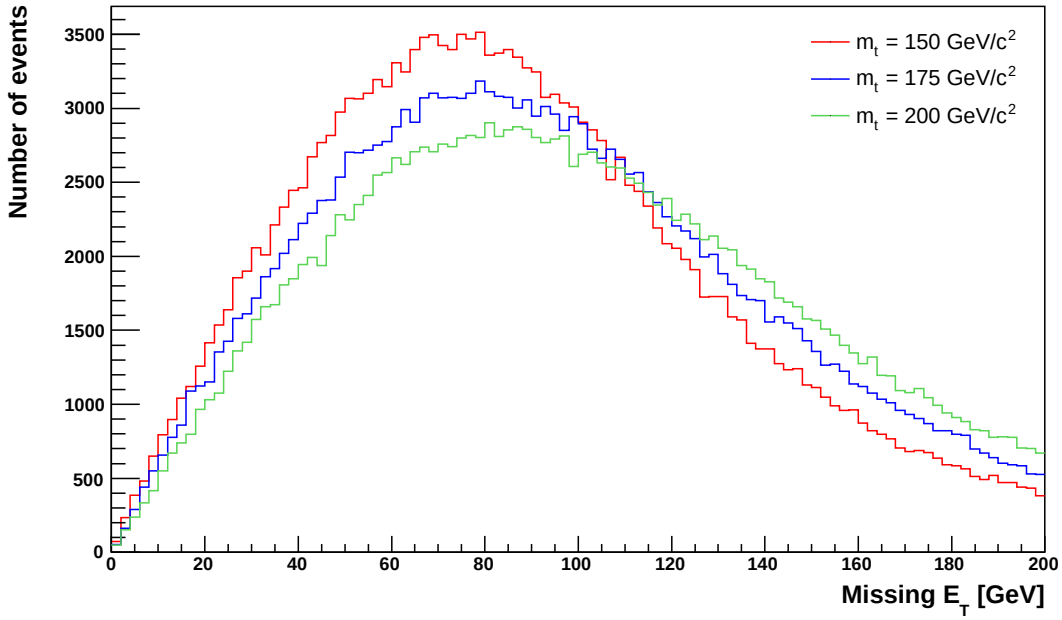

Figure 7.5: Transverse momentum distribution in 'dilepton' events

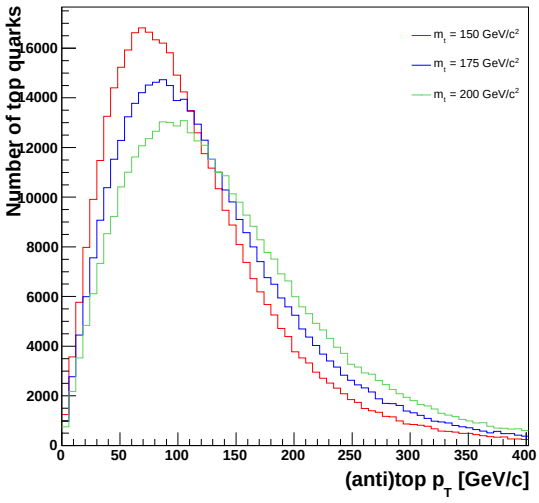

a) top quarks

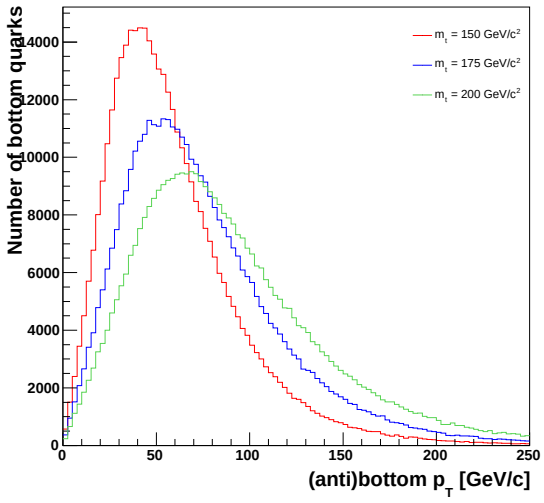

b) bottom quarks

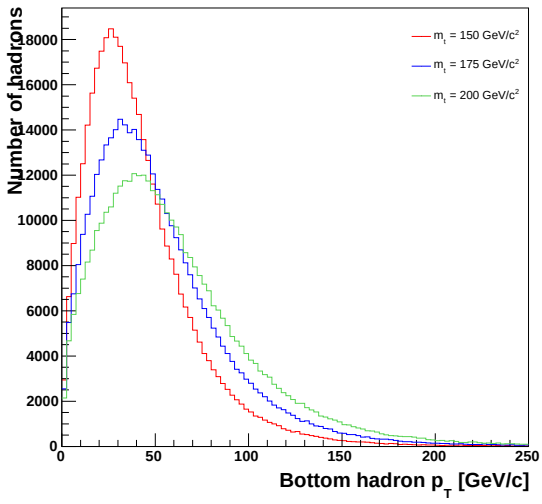

c) bottom hadrons

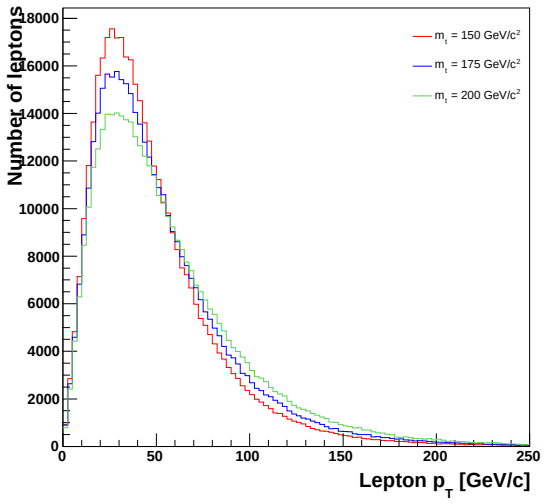

d) leptons

Figure 7.6: Pseudorapidity distribution in 'dilepton' events

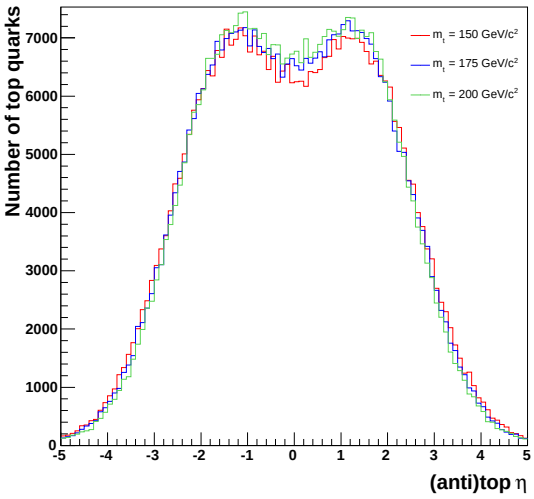

a) top quarks

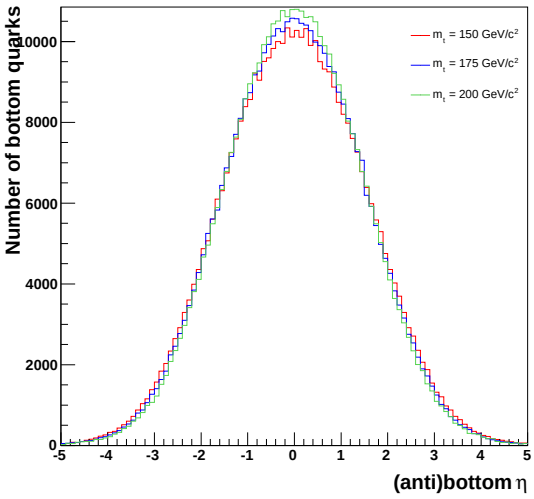

b) bottom quarks

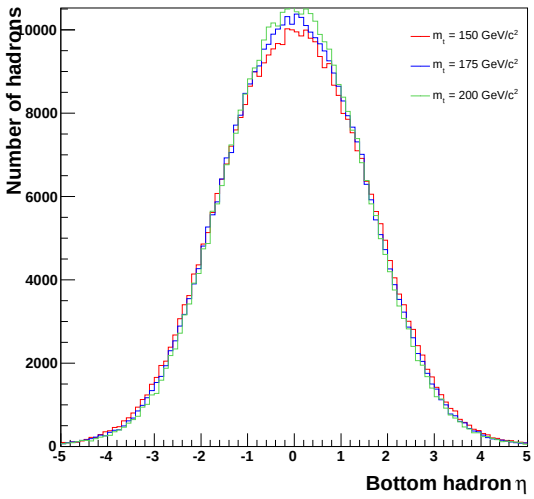

c) bottom hadrons

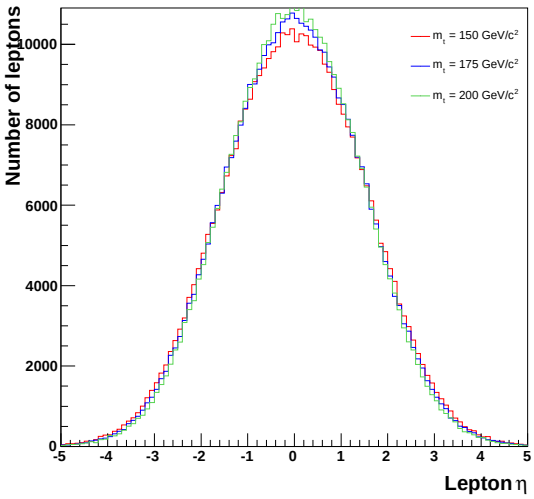

d) leptons

God does not play dice with the universe; He plays an ineffable game of his own devising, which might be compared, from the perspective of any of the other players, to being involved in an obscure and complex version of poker in a pitch dark room, with blank cards, for infinite stakes, with a dealer who won't tell you the rules, and who smiles all the time.

Terry Pratchett

Chapter 8

The Transverse Decay Length of Bottom Hadrons

8.1 L_{xy} from Pythia Events

From each event we selected both b and $\bar{b}$ quark – their first occurrence as non-documentation particles to be more precise.[1] After that we traced the (anti)bottom quark down the decay tree from the fragmentation process ('hidden' in strings) to the decay of the last bottom hadron (bottom hadrons be easily recognized by their PDG code containing the digit '5'). The position of decay vertex is taken from one of the child particles of the last hadron. L_{xy} is the transverse distance between this vertex and the primary interaction vertex.

Histograms of L_{xy} for three different masses (150, 175 and 200 GeV/c^2) are plotted in figure 8.1. As can be seen this distribution is roughly exponential – the agreement would be almost perfect for one precise p_{T} of bottom hadrons.[2]

Because the simulated data samples were small, a parametrization of L_{xy} distribution with as few parameters as possible was needed. Of these, only the mean value itself and exponential fit suited our purpose.

Lognormal distribution was also tested. It successfully fitted individual histograms of L_{xy} from full simulation (see figure 8.4) but the parameters

[1] Pythia divides the list of particles into three parts – particles appearing in the primary interaction (documentation particles), intermediate particle states used in the fragmentation model of Pythia and finally 'real' particles (leptons, hadrons, intermediate bosons) travelling and decaying at reasonable distances from the point of primary interaction. The first occurrence of bottom quark in fragmentation was used because documentation particles do not have information about their daughters attached.

[2] In fact the theoretical distribution of decay lengths for one p_{T} is a sum of several exponential functions because each type of bottom hadrons has different mean lifetime τ. However this effect is inferior to that of the continuous p_{T} spectrum.

Figure 8.1: L_{xy} distribution for different top quark masses (Pythia events)

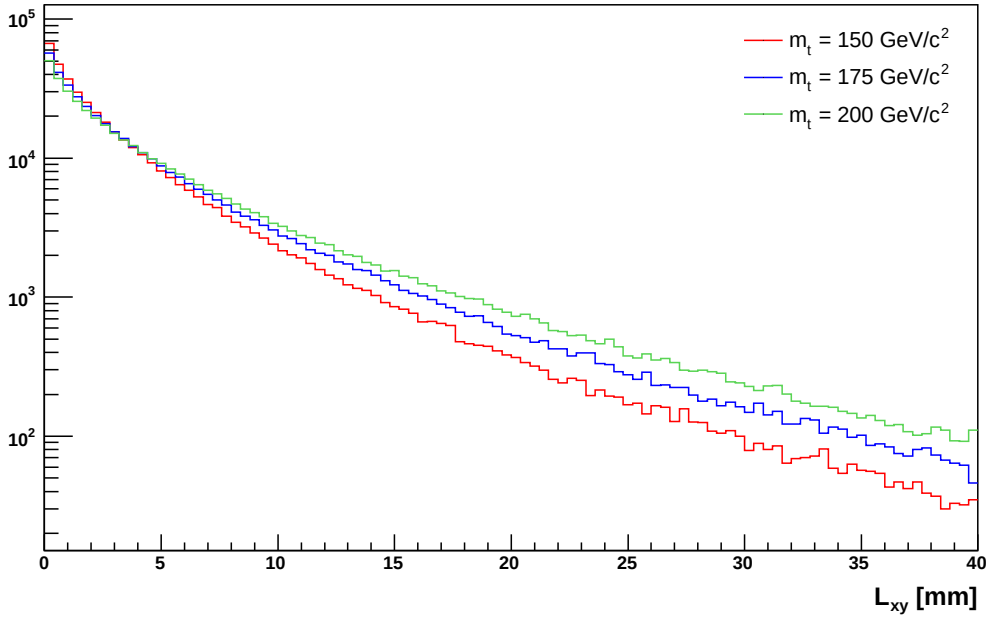

(one additional is needed) were not consistent over the range of masses and even attempts to fix one of them to some definite value led to no satisfactory result.

8.1.1 Parametrization Using the Mean Value

The most natural parametrization is the mean value $\langle L_{xy} \rangle$ itself. It was calculated over several ranges because of the difference in the distribution shape between events from Pythia and from full simulation. Range $(0, \infty)$ is the ideal choice with calculated value being closest to the physical meaning of mean transverse decay length. Other ranges try to avoid problems in the area of low decay lengths, two of them additionally do not contain entries from the long histogram tail.

The statistical uncertainty was set to:

$$\sigma\langle L_{xy} \rangle = \sqrt{\frac{\mathrm{Var}(L_{xy})}{N}}, \tag{8.1}$$

where N is the count of entries and $\mathrm{Var}(L_{xy})$ is their variance. Calculated parameters of Pythia samples with different masses are listed in table 8.1 and plotted in figure 8.2.

Table 8.1: $\langle L_{xy} \rangle$ - mean over selected range for different m_t's (Pythia events). All values are given in mm's.

m_t [GeV/c^2]	Range (0, ∞)	Range (5, ∞)	Range (3, 20)	Range (5, 25)
150	3.632 ± 0.008	10.689 ± 0.025	6.916 ± 0.010	9.529 ± 0.015
155	3.836 ± 0.009	10.918 ± 0.025	7.037 ± 0.010	9.639 ± 0.015
160	3.998 ± 0.009	11.126 ± 0.025	7.116 ± 0.010	9.760 ± 0.015
165	4.152 ± 0.010	11.315 ± 0.026	7.169 ± 0.010	9.834 ± 0.015
170	4.336 ± 0.010	11.490 ± 0.026	7.264 ± 0.010	9.919 ± 0.014
175	4.505 ± 0.010	11.698 ± 0.026	7.334 ± 0.010	9.988 ± 0.014
180	4.668 ± 0.011	11.888 ± 0.026	7.418 ± 0.010	10.087 ± 0.014
185	4.818 ± 0.011	12.054 ± 0.026	7.454 ± 0.010	10.149 ± 0.014
190	4.983 ± 0.011	12.229 ± 0.026	7.549 ± 0.010	10.230 ± 0.014
195	5.141 ± 0.012	12.423 ± 0.027	7.588 ± 0.010	10.269 ± 0.014
200	5.305 ± 0.012	12.573 ± 0.027	7.655 ± 0.010	10.341 ± 0.014

8.1.2 Parametrization Using the Exponential Fit

ROOT built-in fitting capabilities were used for fitting the histograms over several finite-length intervals with an exponential function:

$$f(x) = a \cdot e^{-\frac{1}{b}x}, \tag{8.2}$$

where a and b are parameters of the fit. In the following we take b as our estimation of $\langle L_{xy} \rangle$. The ranges were selected with respect to the shape of histograms from full simulation. Interval (0, 15) gives the most precise fit of Pythia samples but it is of no use for data from full simulation. Other three ranges to some extent avoid the problems with identifying vertices near beam axis.

The parameters are listed in table 8.2 and plotted in figure 8.3.

Figure 8.2: $\langle L_{xy} \rangle$ - mean over selected range (Pythia events)

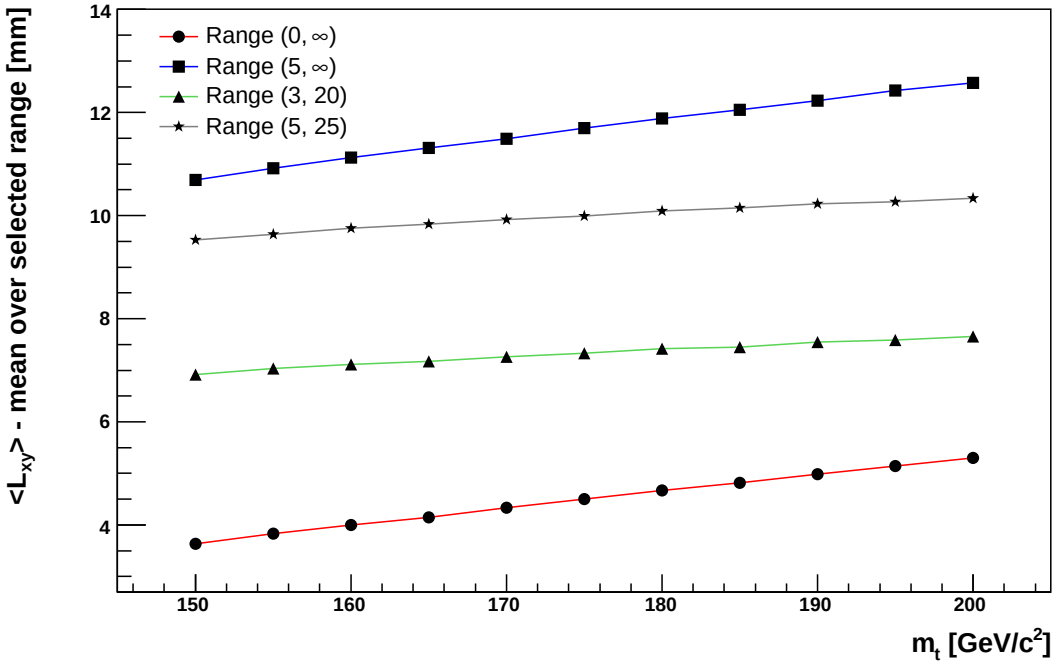

Table 8.2: $\langle L_{xy} \rangle$ - exponential fit over selected range for different m_t's (Pythia events). All values are given in mm's.

m_t [GeV/c^2]	Range (0, 15)	Range (4, 15)	Range (5, 20)	Range (5, 25)
150	2.907 ± 0.007	4.137 ± 0.021	4.626 ± 0.023	4.818 ± 0.022
155	3.036 ± 0.007	4.301 ± 0.022	4.774 ± 0.024	4.977 ± 0.022
160	3.132 ± 0.008	4.431 ± 0.023	4.938 ± 0.025	5.155 ± 0.023
165	3.226 ± 0.008	4.506 ± 0.024	5.029 ± 0.025	5.266 ± 0.023
170	3.350 ± 0.008	4.654 ± 0.024	5.138 ± 0.025	5.388 ± 0.023
175	3.451 ± 0.008	4.758 ± 0.025	5.283 ± 0.026	5.515 ± 0.024
180	3.539 ± 0.009	4.882 ± 0.026	5.442 ± 0.027	5.680 ± 0.024
185	3.622 ± 0.009	4.927 ± 0.026	5.476 ± 0.027	5.768 ± 0.025
190	3.723 ± 0.009	5.108 ± 0.028	5.653 ± 0.028	5.916 ± 0.025
195	3.809 ± 0.010	5.200 ± 0.028	5.728 ± 0.028	5.990 ± 0.025
200	3.906 ± 0.010	5.263 ± 0.028	5.818 ± 0.029	6.112 ± 0.026

Figure 8.3: Exponential fit of $\langle L_{xy} \rangle$ for different masses (Pythia events)

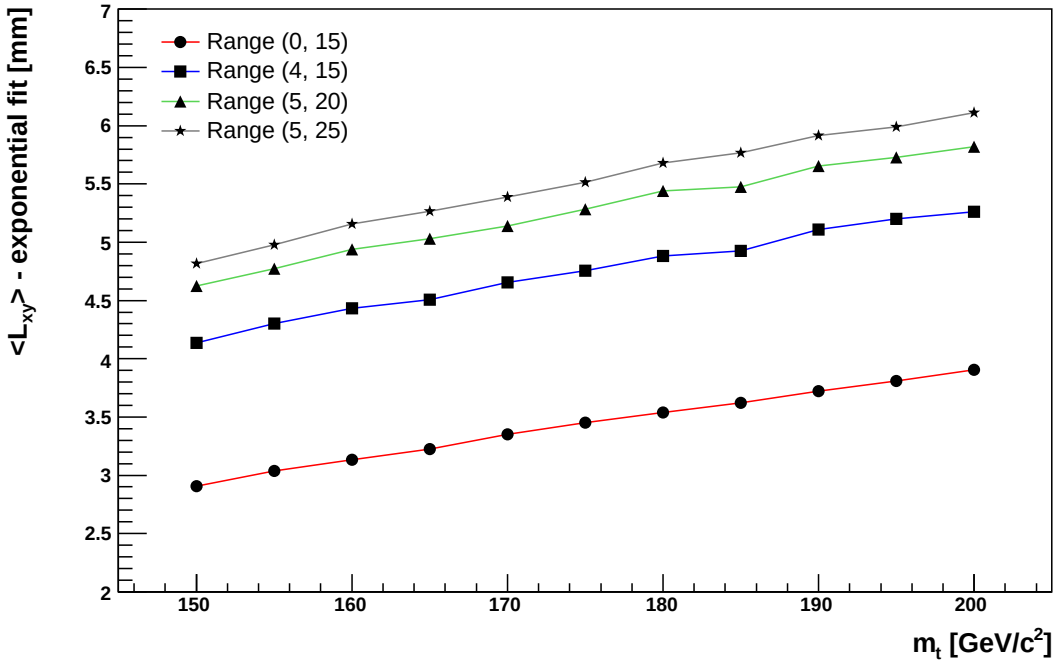

Figure 8.4: L_{xy} spectra for different top quark masses (full simulation)

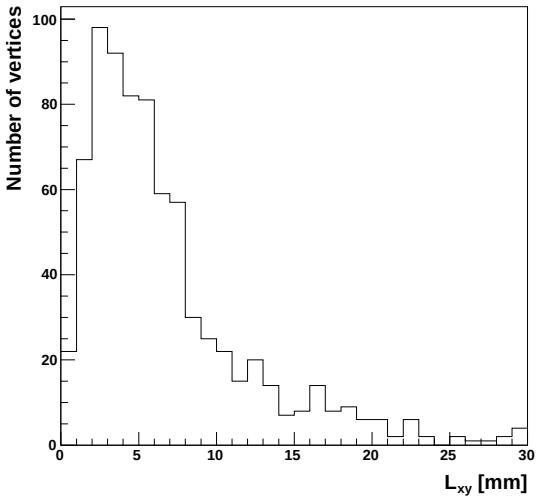

$m_t = 165$ GeV/c^2

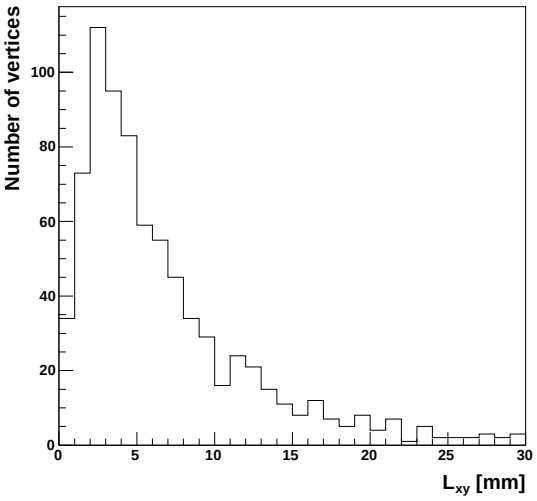

$m_t = 170$ GeV/c^2

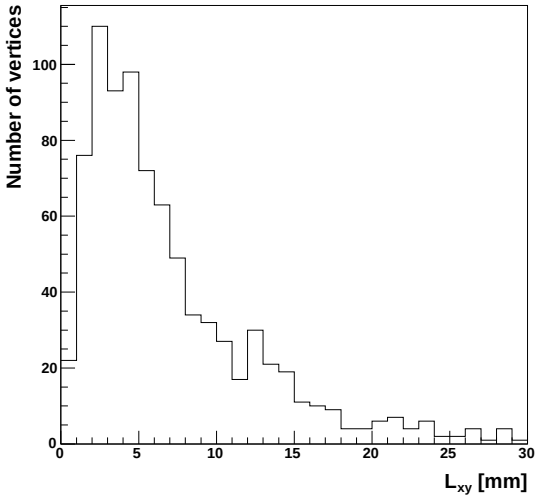

$m_t = 175$ GeV/c^2 (11.0.4 sample)

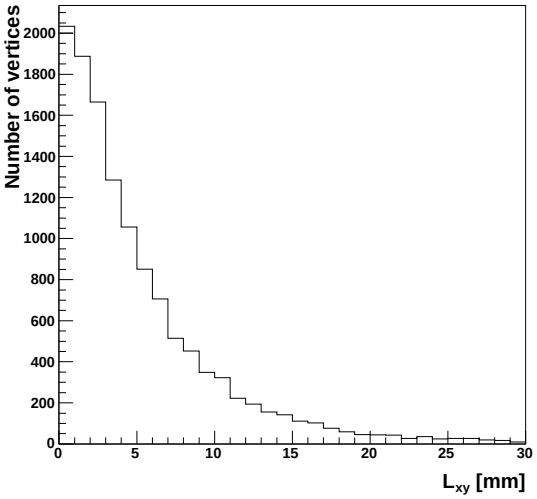

$m_t = 175$ GeV/c^2 (Rome sample 4522)

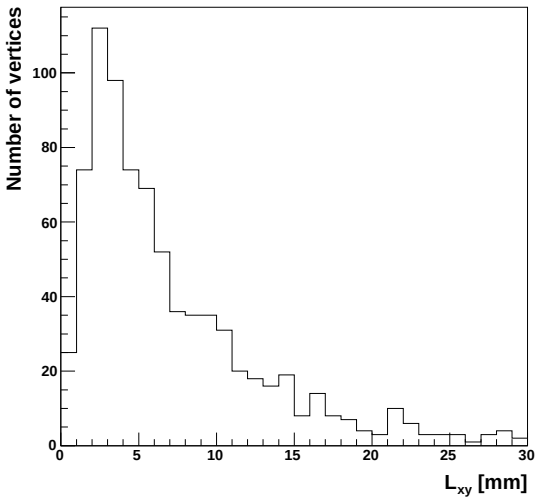

$m_t = 180$ GeV/c^2

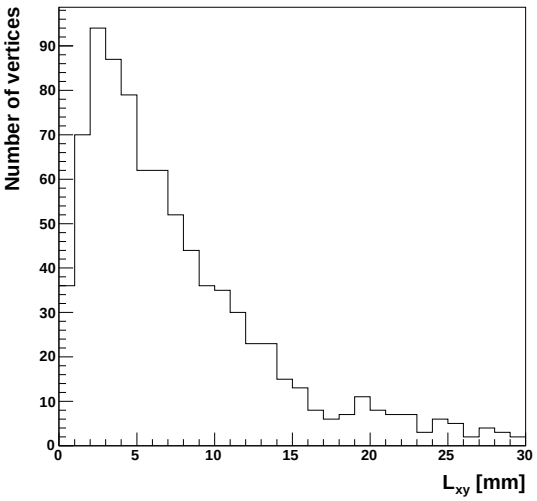

$m_t = 185$ GeV/c^2

8.2 L_{xy} from Full-Simulation Events

The transverse decay lengths of bottom hadrons were obtained from `SecVtxBU` tagging info appended to corresponding jets. We selected only jets that that occurred in events fulfilling our loosened criteria, which had the tagging likelihood of more than 0.9.

The histograms of transverse decay length are plotted in figure 8.4. As can be easily spotted, Rome sample differs substantially from the customized samples. Because the hadrons generated by Monte Carlo generators should have similar exponential distributions of transverse decay lengths (a proof would be useful here) and because the selection algorithms were identical (although compiled with different version of Athena framework), we account this discrepancy to subtle changes in tagging algorithms used in release 10 and 11 of Atlas offline software or some non-default settings used in reconstruction of the Rome sample [3] Nevertheless it should be noted here that for any reasonable analysis it is absolutely necessary that we could rely on the consistence of results obtained by b-tagging algorithms on different data samples. In the following we assume that our data can be trusted (they are indeed consistent – the whole simulation process was identical but for a change of one parameter), however this study has to be repeated in newer releases of Atlas software.[4]

We also compare the L_{xy} distributions of samples from both Pythia and our customized full simulation in figure 8.5.

The parametrization used for the description of L_{xy} was identical to that used in the previous section. We list the parameters in tables 8.3 and 8.4. They are plotted in figures 8.7 and 8.6. A detailed discussion of individual parametrizations follows in the next section.

8.3 Suitable Parametrizations

The choice of parametrization is inevitably connected with the matter of statistical and systematic uncertainties. Parameters used in the place of physical $\langle L_{xy} \rangle$ differ in degree to which they are sensible to the variation of top quark mass. The greater the relative change the better we can manage the uncertainties.

[3] In fact the low number of vertices near the beam line is in favour of the customized samples due to the detector resolution and the density of tracks. Similar distribution was obtained in [11].

[4] Reconstruction algorithms in release 12 have not yet been validated for general use.

Figure 8.5: L_{xy} distributions of samples from both Pythia and full simulation. The histograms are normalized.

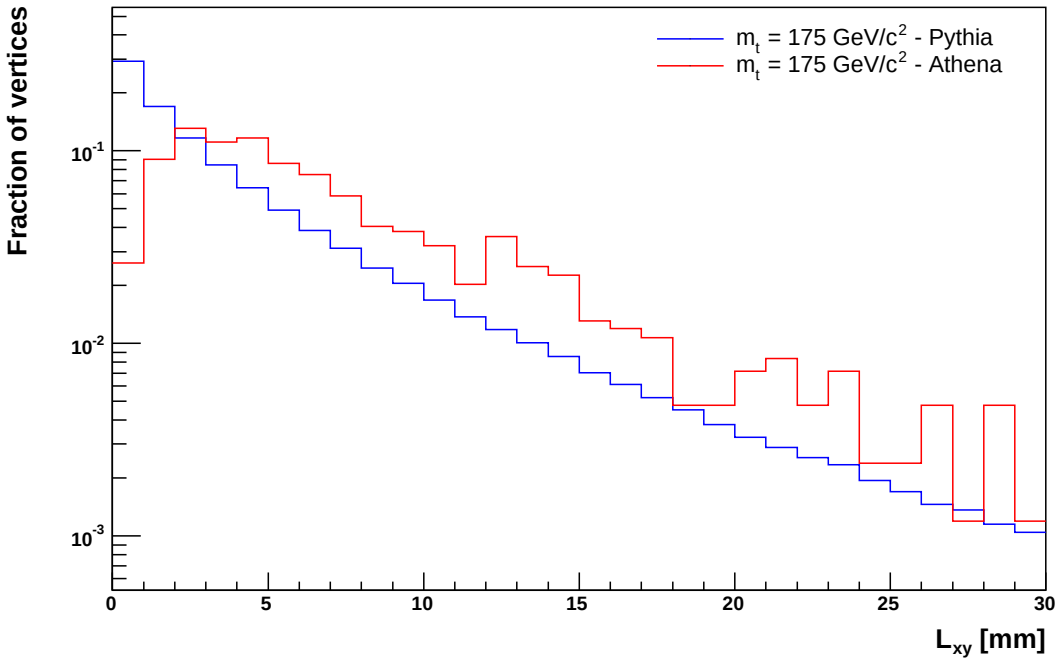

The comparison between parameters obtained from Pythia and full-simulation data is plotted in figures 8.8 to 8.11. We fitted $\langle L_{xy} \rangle$-like values obtained for individual top quark masses with a linear function in ROOT. The use of linear fitting is justified by figures 8.2 and 8.3. The slopes of these fits are listed in table 8.5.

We required that the slope of full-simulation parametrization was within the range of one standard deviation from the slope of Pythia dependence. Further we ruled out mean over the range $(0, \infty)$ – although the slope seems to be all right, $\langle L_{xy} \rangle$ values obtained this way are dependent on the shape of peak present in the spectrum and this should be avoided.

Thus we were left with four different parametrizations – two of them being means and two of them obtained as parameters of exponential distribution. The top quark mass can be obtained from these equations:[5]

$$m_t \ [\mathrm{GeV}/c^2] = 175 + (\langle L_{xy} \rangle_5^{\infty} \ [\mathrm{mm}] - 12.33) \times 0.062 \qquad (8.3)$$

[5]For brevity we mark mean over the range of (a, b) as $\langle L_{xy} \rangle_a^b$ and the parameter of exponential fit over the same interval as $\langle l_{xy} \rangle_a^b$.

Table 8.3: $\langle L_{xy} \rangle$ - mean over selected range for different m_t's (full simulation). All values are given in mm's.

Sample	Range (0, ∞)	Range (5, ∞)	Range (3, 20)	Range (5, 25)
165 GeV/c^2	7.59 ± 0.32	11.64 ± 0.51	7.58 ± 0.17	9.75 ± 0.23
170 GeV/c^2	7.43 ± 0.29	12.08 ± 0.47	7.67 ± 0.18	10.22 ± 0.24
175 GeV/c^2	7.94 ± 0.30	12.31 ± 0.46	7.72 ± 0.16	10.23 ± 0.22
180 GeV/c^2	8.04 ± 0.35	12.72 ± 0.58	7.82 ± 0.18	10.43 ± 0.24
185 GeV/c^2	8.56 ± 0.43	12.84 ± 0.68	8.07 ± 0.17	10.54 ± 0.22
Rome 4522	5.49 ± 0.06	11.07 ± 0.13	7.33 ± 0.05	9.68 ± 0.07

Table 8.4: $\langle L_{xy} \rangle$ - exponential fit over selected range for different m_t's (full simulation). All values are given in mm's.

Sample	Range (0, 15)	Range (4, 15)	Range (5, 20)	Range (5, 25)
165 GeV/c^2	11.4 ± 1.0	4.21 ± 0.31	4.44 ± 0.37	4.74 ± 0.38
170 GeV/c^2	10.6 ± 0.9	4.86 ± 0.45	5.35 ± 0.46	5.61 ± 0.45
175 GeV/c^2	16.4 ± 2.1	5.17 ± 0.50	5.03 ± 0.36	5.28 ± 0.34
180 GeV/c^2	18.1 ± 2.6	5.85 ± 0.64	5.23 ± 0.40	5.45 ± 0.38
185 GeV/c^2	13.6 ± 1.4	6.18 ± 0.62	5.31 ± 0.38	5.44 ± 0.34
Rome 4522	5.02 ± 0.06	4.74 ± 0.12	4.89 ± 0.11	5.02 ± 0.10

$$m_t \ [\mathrm{GeV}/c^2] = 175 + (\langle L_{xy} \rangle_3^{20} \ [\mathrm{mm}] - 7.77) \times 0.023 \tag{8.4}$$

$$m_t \ [\mathrm{GeV}/c^2] = 175 + (\langle l_{xy} \rangle_5^{20} \ [\mathrm{mm}] - 5.03) \times 0.036 \tag{8.5}$$

$$m_t \ [\mathrm{GeV}/c^2] = 175 + (\langle l_{xy} \rangle_5^{25} \ [\mathrm{mm}] - 5.28) \times 0.027 \tag{8.6}$$

A combination of these parametrizations could possibly provide us with more precise results as the mean value and the shape of exponential fit are not totally correlated. Other parametrizations may also prove useful, however this is beyond the scope of this work. We present the statistical error of individual equations in the next section.

Figure 8.6: Exponential fit of $\langle L_{xy} \rangle$ for different masses (full simulation)

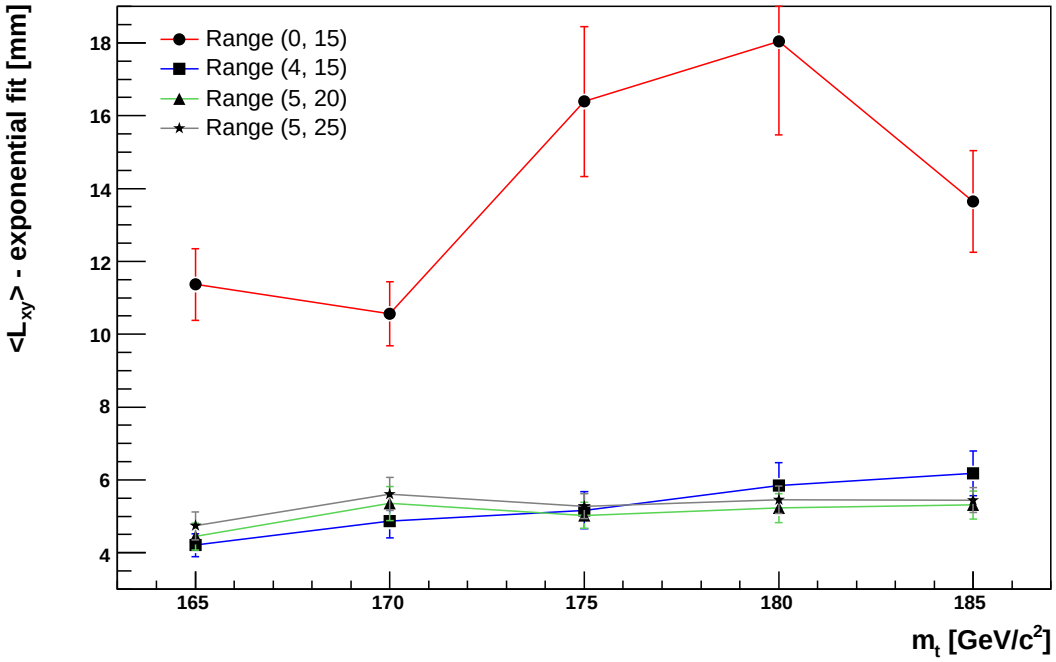

8.4 Statistical Uncertainty

The statistical errors of equations in the previous section were obtained by dividing the uncertainty of a single point (the one associated with $m_t = 175$ GeV/c^2) in the plot by the slope of its linear fit.[6] Both parametrization using mean have a statistical uncertainty of 7 GeV/c^2, exponential fits have statistical errors of 10 GeV/c^2 in the case of $\langle l_{xy} \rangle_5^{20}$ and 13 GeV/c^2 in the case of $\langle l_{xy} \rangle_5^{20}$. Statistical uncertainties estimated for the amounts of data collected at ATLAS are discussed in section 8.6.

[6] It is a simplification but it satisfies our requirement of a rough estimation in the investigated range of masses.

Figure 8.7: $\langle L_{xy} \rangle$ - mean over selected range (full simulation)

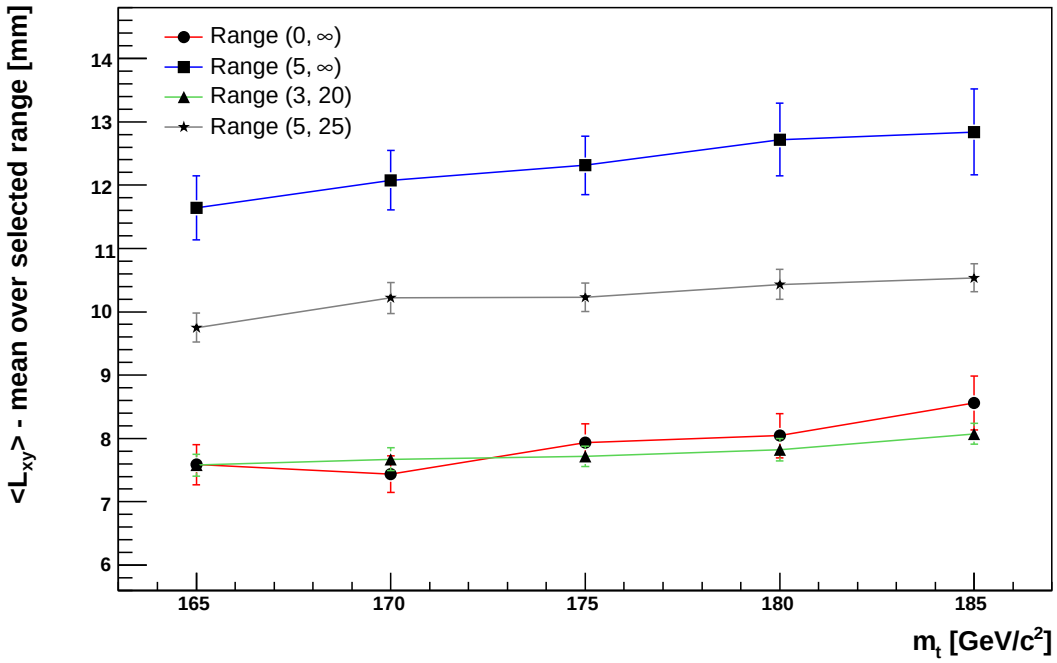

Table 8.5: Dependence of $\langle L_{xy} \rangle$-like parameters on m_t - slope of the linear fit. All values are given in mm's.

Parameter	Pythia	Full simulation
Mean L_{xy} over selected range [mm]		
Range (0, ∞)	0.034 ± 0.001	0.049 ± 0.022
Range (5, ∞)	0.038 ± 0.002	0.062 ± 0.036
Range (3, 20)	0.015 ± 0.001	0.023 ± 0.011
Range (5, 25)	0.016 ± 0.001	0.036 ± 0.014
Exponential fit over selected range [mm]		
Range (0, 15)	0.020 ± 0.001	0.194 ± 0.081
Range (4, 15)	0.022 ± 0.002	0.100 ± 0.030
Range (5, 20)	0.024 ± 0.002	0.036 ± 0.024
Range (5, 25)	0.026 ± 0.002	0.027 ± 0.023

Figure 8.8: Mean L_{xy} for different masses – comparison of Athena and Pythia events.

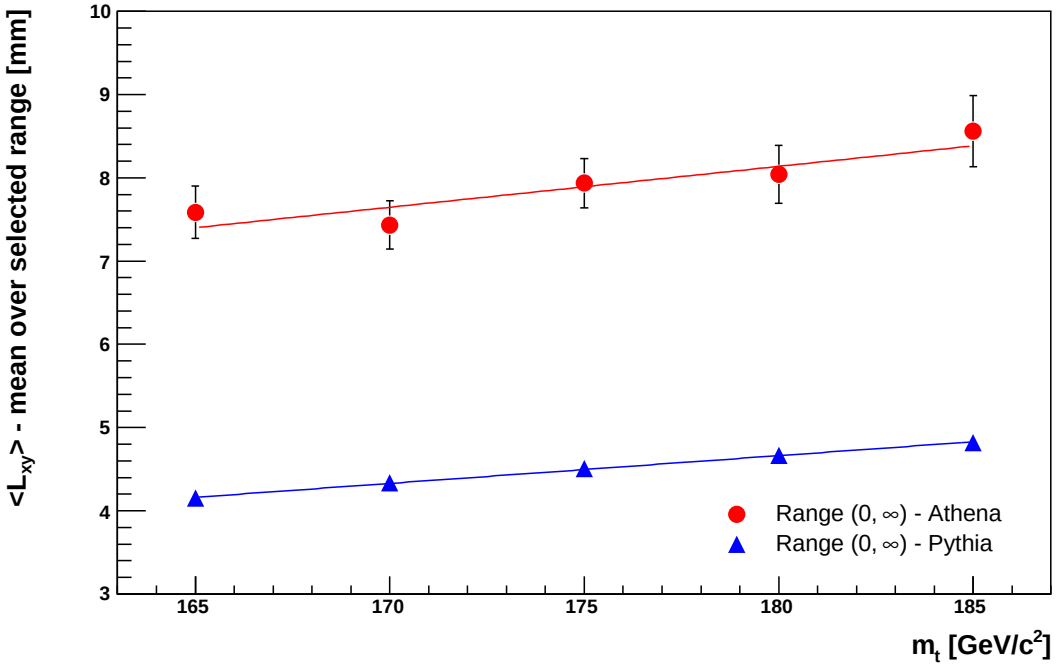

a) Range (0, ∞)

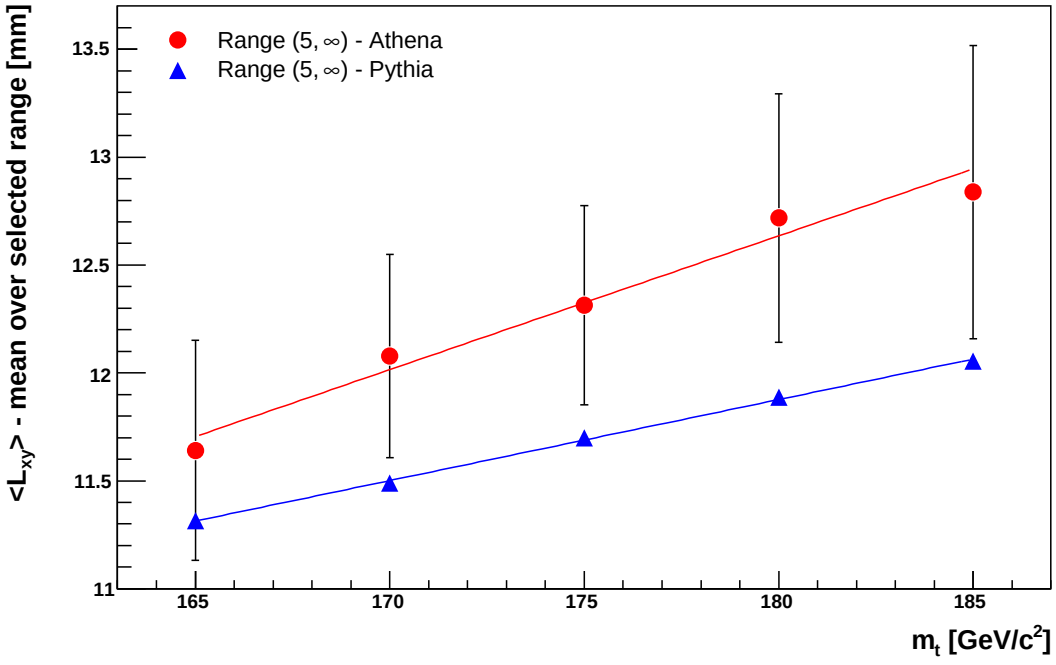

b) Range (5, ∞)

Figure 8.9: Mean L_{xy} for different masses – comparison of Athena and Pythia events.

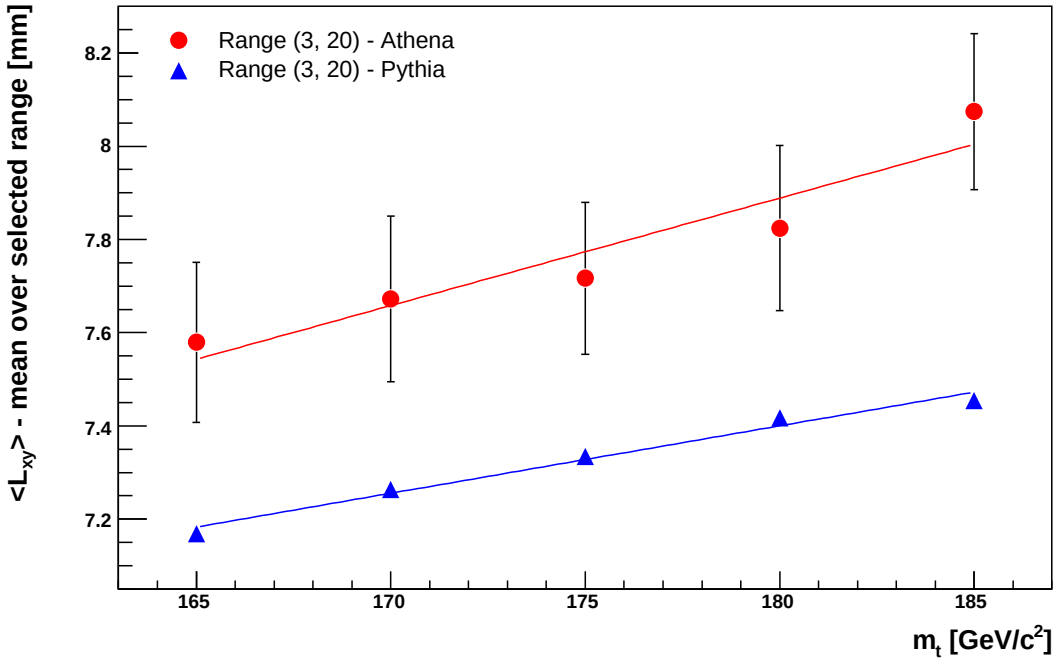

a) Range (3, 20)

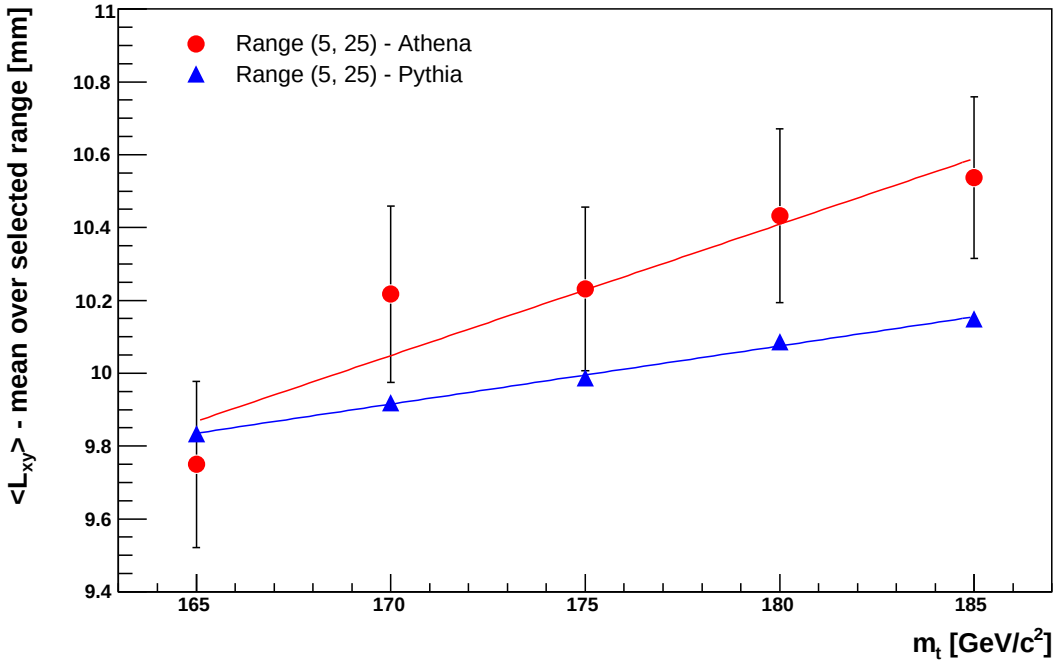

b) Range (5, 25)

Figure 8.10: Exponential fit of L_{xy} for different masses – comparison of Athena and Pythia events.

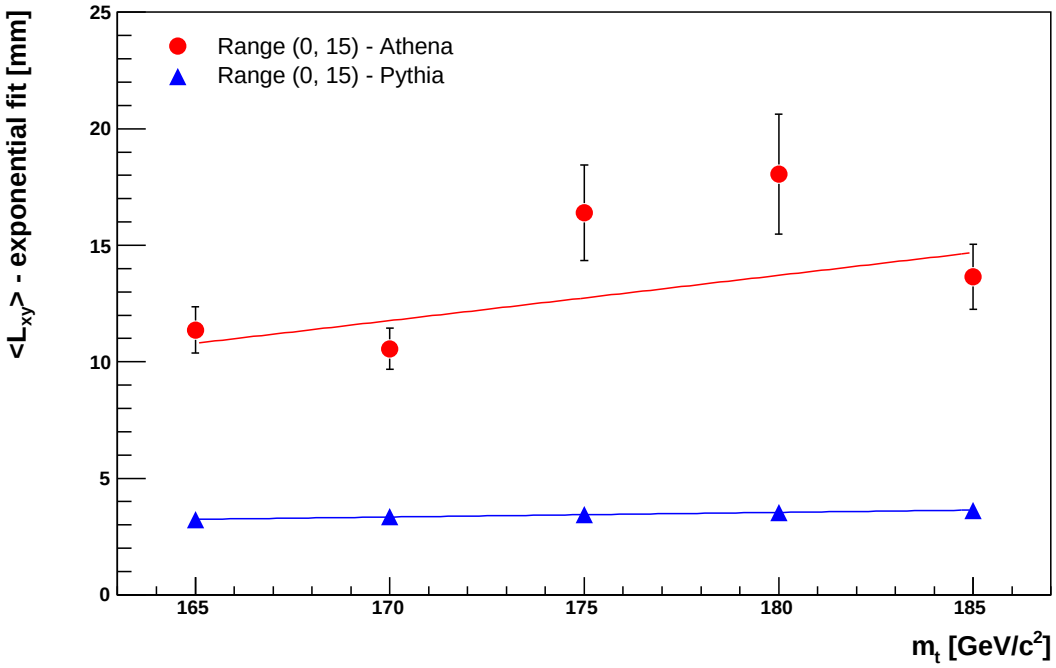

a) Range (0, 15)

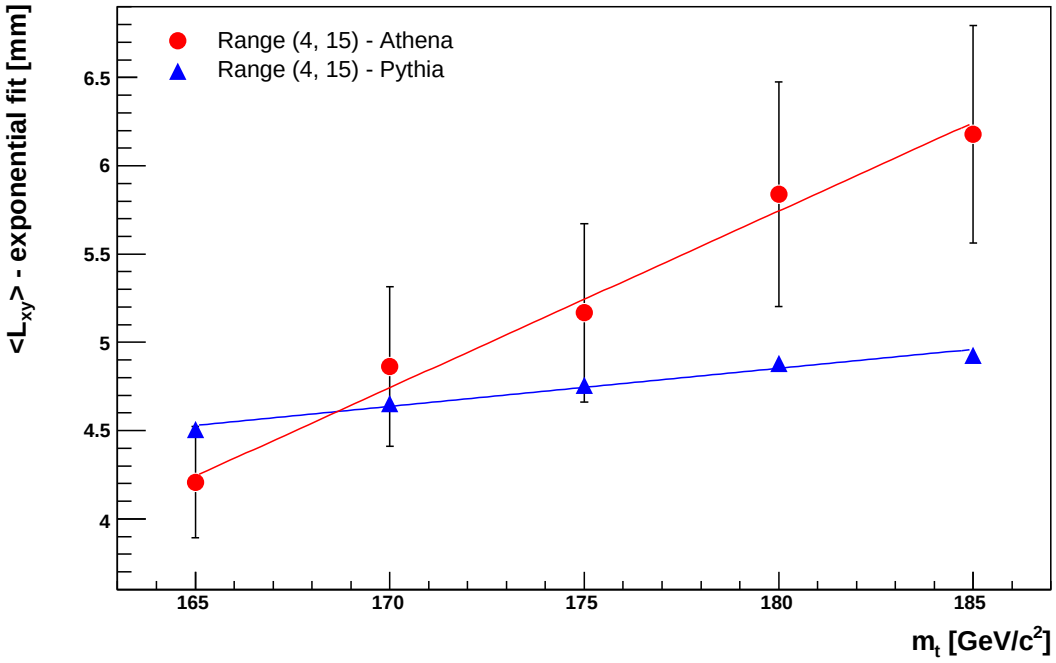

b) Range (4, 15)

Figure 8.11: Exponential fit of L_{xy} for different masses – comparison of Athena and Pythia events.

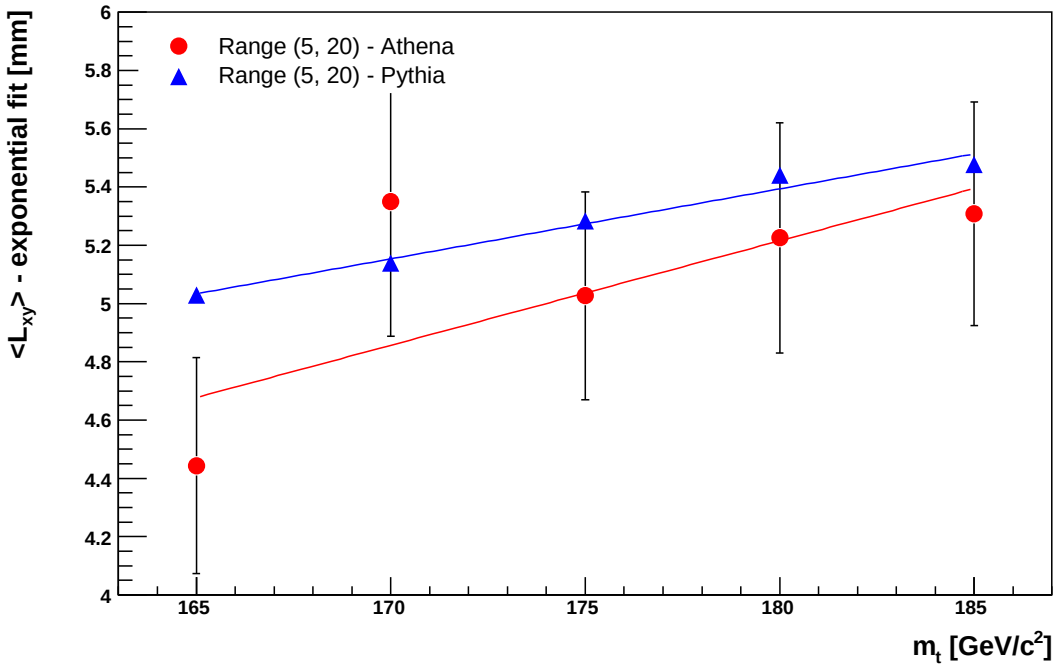

a) Range (5, 20)

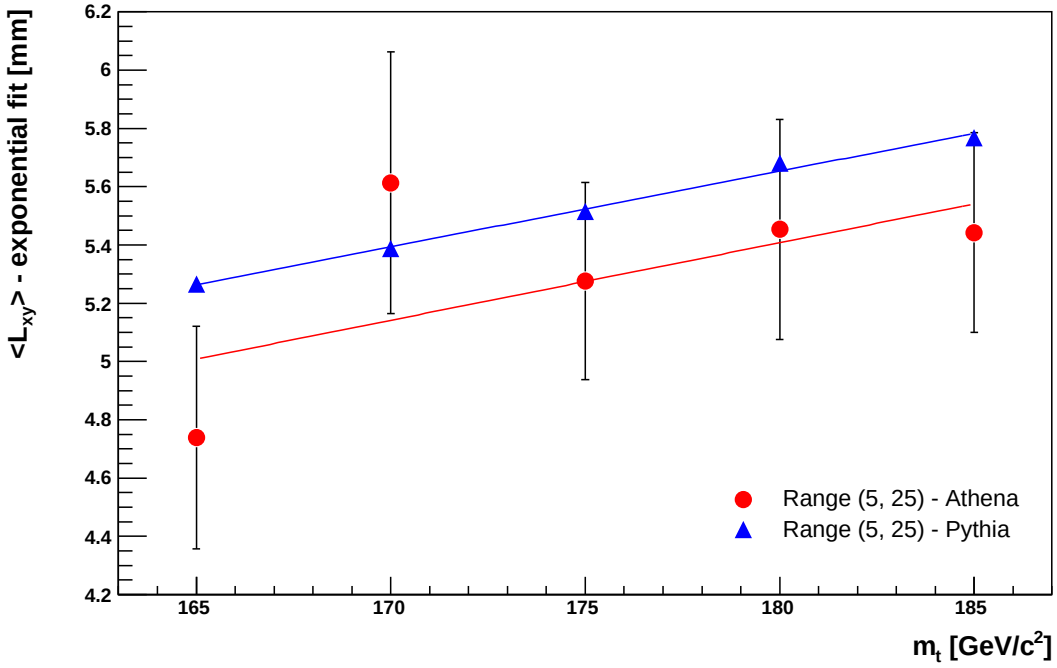

b) Range (5, 25)

8.5 Systematic Uncertainties

Main part of the uncertainties investigation was done in Pythia as we did not expect them to be distinguishable in our limited samples from full simulation. We generated additional samples with the top quark mass $m_t = 175$ GeV/c^2 of the same size as the default one (i.e. 200,000 events[7]) using the same Pythia configuration with a change just in the settings of the studied matter. We believe that the relative uncertainty obtained from Pythia samples can be applied on simulated (or measured) data.

The systematic error due to this change was calculated for each of the selected parametrizations – again we divided the shift of $\langle L_{xy} \rangle$ by the slope of the parametrization (obtained from Pythia samples). Often the change was negligible with respect to the uncertainty of the parameter, so only an upper limit for the resulting systematic error in mass measurement was put.

8.5.1 Parton Distribution Functions

We used the main sample of Pythia-generated data for the top quark mass of 175 GeV/c^2, which employs the CTEQ5L PDFs, and two modified samples employing CTEQ5M1 and GRV94M parton distribution functions. The parameters of Pythia were identical but for this choice.

The histograms of transverse decay length are plotted in figure 8.14. The parameters fitted from the modified samples are listed in table 8.9 as well as the estimated systematic uncertainties (we chose the more pessimistic GRV94M PDF set for this estimation).

More complex approach proposed by the CTEQ collaboration uses 41 CTEQ6M sets of PDFs with both positive end negative modifications of 20 independent parameters. This method was investigated by [20] but it is beyond the scope of this work.

8.5.2 The Lifetime of Bottom Hadrons

Current experimental values of mean lifetimes of important bottom hadrons [41][42] are listed in table 8.7 along with their fraction in our samples.[8]

The weighted average of mean lifetimes is used for a simple theoretical prediction, the individual mean lifetimes were used as input values for two

[7] or 400,000 transverse decay lengths

[8] By that we mean the fraction of final bottom hadrons whose decay vertices are analysed in this work.

Table 8.6: $\langle L_{xy} \rangle$ fit parameters from samples with different parton distribution function sets ($m_t = 175$ GeV/c^2)

PDF	CTEQ5L	CTEQ5M1	GRV94M	Δm_t [GeV/c^2]
Mean L_{xy} over selected range [mm]				
Range (0, ∞)	4.505 ± 0.010	4.523 ± 0.010	4.491 ± 0.010	—
Range (5, ∞)	11.698 ± 0.026	11.785 ± 0.027	11.678 ± 0.026	2.4
Range (3, 20)	7.334 ± 0.010	7.332 ± 0.010	7.340 ± 0.010	< 0.7
Range (5, 25)	9.988 ± 0.014	10.023 ± 0.014	10.013 ± 0.014	—
Exponential fit over selected range [mm]				
Range (0,15)	3.451 ± 0.008	3.436 ± 0.008	3.439 ± 0.008	—
Range (4,15)	4.758 ± 0.025	4.762 ± 0.025	4.758 ± 0.025	—
Range (5,20)	5.283 ± 0.026	5.291 ± 0.026	5.301 ± 0.026	< 1.0
Range (5,25)	5.515 ± 0.024	5.559 ± 0.024	5.548 ± 0.024	1.7

samples with minimal and maximal bottom hadron lifetime.

Table 8.7: Bottom Hadron Mean Lifetime

Hadron	Fraction (%)	Mean Lifetime (10^{-12} s)
B^0	39.5	1.530 ± 0.009
$B^\pm$	39.5	1.638 ± 0.011
B_s^0	11.8	1.466 ± 0.059
$B_c^\pm$	0.01	0.46 ± 0.18
η_b	~ 0.0002	?
Υ	~ 0.001	1.3×10^{-8}
Λ_b^0	7.9	1.230 ± 0.074
Ξ_b^0	0.5	1.39 ± 0.34
$\Xi_b^\pm$	0.5	1.39 ± 0.34
$\Omega_b^\pm$	0.01	?
Average	—	1.568 ± 0.009

The relative uncertainty of the averaged mean lifetime is 0.58 %. Because of the linear dependence of *physical* $\langle L_{xy} \rangle$ on the lifetime (see equation 3.2) we estimate that our parametrizations are as sensitive to the averaged bottom hadron lifetime as they are sensitive to $\langle L_{xy} \rangle$ itself and therefore the associated systematic error should be independent of the parametrization choice. We estimate the error from $\langle L_{xy} \rangle_0^\infty$ parametrization to be 0.7 GeV/c^2.

The histograms of transverse decay length are plotted in figure 8.13. The

Figure 8.12: The influence of parton distribution functions choice on L_{xy}

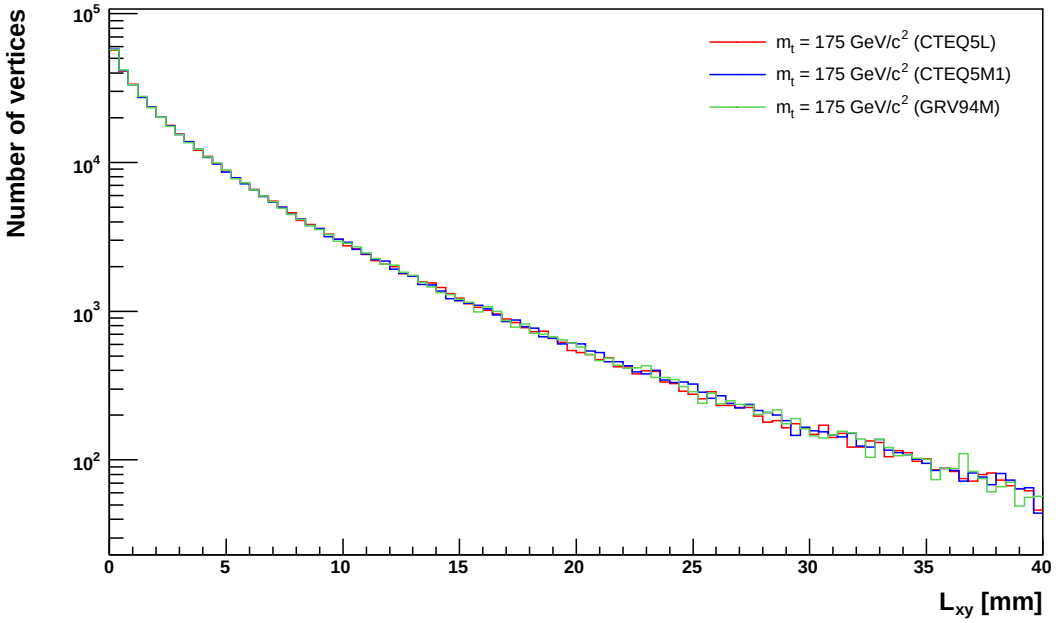

parameters obtained from our samples are listed in table 8.8 – as differences are asymmetrical, we used their average value as the basis for the evaluation of systematic error. Our errors are more pessimistic than the theoretical prediction.

8.5.3 Bottom Fragmentation

Our investigation of the influence of bottom fragmentation on $\langle L_{xy} \rangle$ is similar to that of the authors of [19]. We generated a sample in Pythia for $m_t = 175$ GeV/c^2 , which had a changed value of the *Peterson parameter*. We shifted it from its default value ($\epsilon_b = -0.005$) by its current uncertainty of 0.0025 to -0.0025.

We did not observe any measurable difference between this sample and the default one. Both spectra of L_{xy} are plotted in figure 8.14. Fit parameters are listed in table 8.9. They do not differ from the default values by more than one standard deviation. Thus we believe the influence of bottom fragmentation to be negligible – however only an upper limit of systematic error was set.

Table 8.8: $\langle L_{xy} \rangle$ fit parameters from samples with modified mean bottom hadron lifetimes ($m_t = 175$ GeV/c^2)

Hadron lifetime	default	minimum	maximum	Δm_t [GeV/c^2]
Mean L_{xy} over selected range [mm]				
Range (0, ∞)	4.505 ± 0.010	4.484 ± 0.010	4.626 ± 0.011	—
Range (5, ∞)	11.698 ± 0.026	11.685 ± 0.026	11.817 ± 0.026	1.8
Range (3, 20)	7.334 ± 0.010	7.326 ± 0.010	7.384 ± 0.010	2.0
Range (5, 25)	9.988 ± 0.014	9.973 ± 0.014	10.039 ± 0.014	—
Exponential fit over selected range [mm]				
Range (0,15)	3.451 ± 0.008	3.434 ± 0.008	3.529 ± 0.009	—
Range (4,15)	4.758 ± 0.025	4.742 ± 0.025	4.821 ± 0.025	—
Range (5,20)	5.283 ± 0.026	5.269 ± 0.026	5.367 ± 0.026	2.1
Range (5,25)	5.515 ± 0.024	5.493 ± 0.023	5.599 ± 0.024	2.0

Table 8.9: $\langle L_{xy} \rangle$ fit parameters from samples with different values of Peterson fragmentation function parameter of bottom quarks ($m_t = 175$ GeV/c^2)

ϵ_b	-0.0050	-0.0025	Δm_t [GeV/c^2]
Mean L_{xy} over selected range [mm]			
Range (0, ∞)	4.505 ± 0.010	4.499 ± 0.010	—
Range (5, ∞)	11.698 ± 0.026	11.690 ± 0.026	< 0.7
Range (3, 20)	7.334 ± 0.010	7.339 ± 0.010	< 0.7
Range (5, 25)	9.988 ± 0.014	9.993 ± 0.014	—
Exponential fit over selected range [mm]			
Range (0,15)	3.451 ± 0.008	3.445 ± 0.008	—
Range (4,15)	4.758 ± 0.025	4.754 ± 0.025	—
Range (5,20)	5.283 ± 0.026	5.292 ± 0.026	< 1.1
Range (5,25)	5.515 ± 0.024	5.526 ± 0.024	< 0.9

Figure 8.13: L_{xy} distribution for samples with modified bottom hadron lifetimes

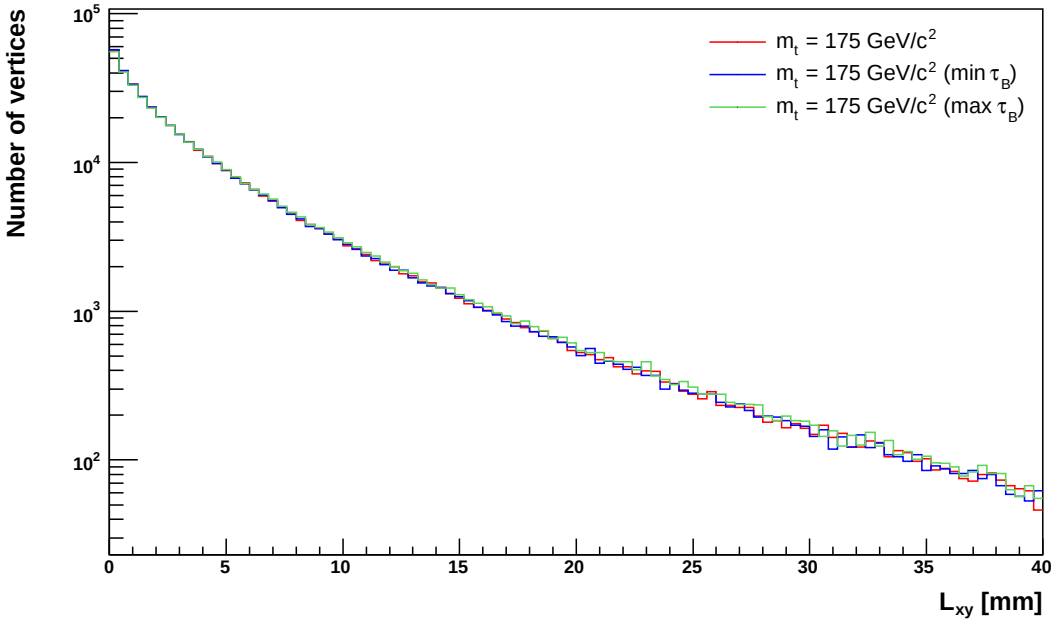

8.5.4 Initial- and Final-State Radiation

Initial-state radiation is responsible for two effects, that can possibly affect mean transverse decay length of bottom hadrons. It can produce additional jets with sufficient energy to get reconstructed. This will however mostly result in the rejection of event. Apart from this, the $t\bar{t}$ pairs can receive non-zero transverse momentum – this is illustrated in figure 8.15, where standard Pythia sample is compared with sample where initial-state radiation is switched off.

Nevertheless this non-zero transverse momentum is negligible when compared to the transverse momentum of individual top quarks and their rest mass, which is the primary source of the bottom quark p_{T}. Thus we did not expect a significant effect.

Both the effects of initial- and final-state radiation on the L_{xy} are plotted in figure 8.16. Fit parameters of the sample with no initial-state radiation are listed in table 8.10. According to [19], initial- and final-state radiation are known to 20 % level and therefore we estimate the systematic errors as one fifth of the shift in mass found in the samples.

Figure 8.14: The influence of bottom fragmentation uncertainties on L_{xy}

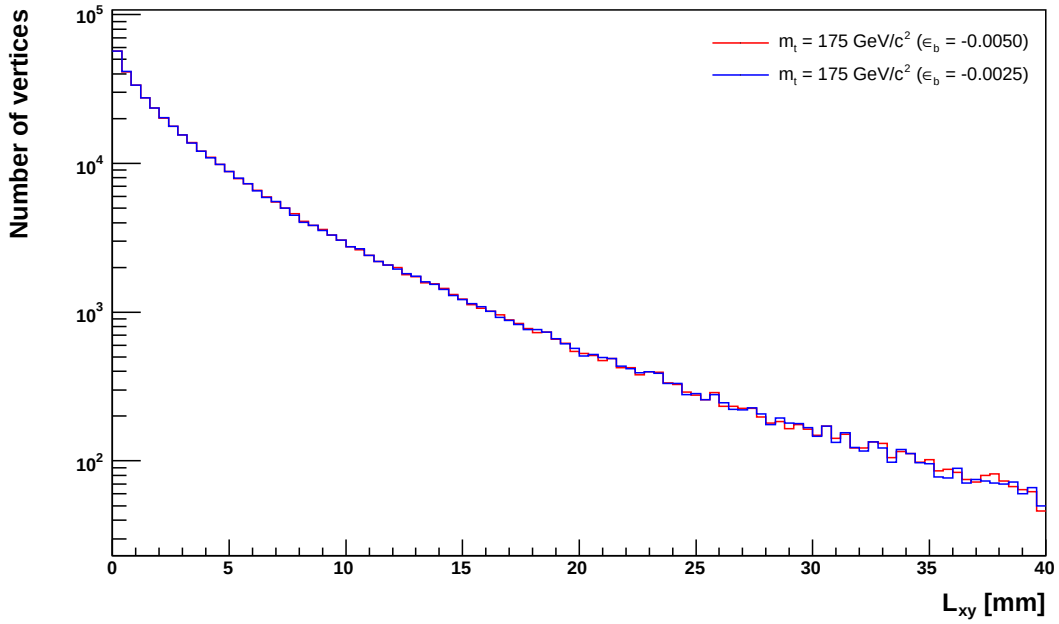

Figure 8.15: Transverse momentum of the $t\bar{t}$ pair. Comparison of samples with and without initial-state radiation.

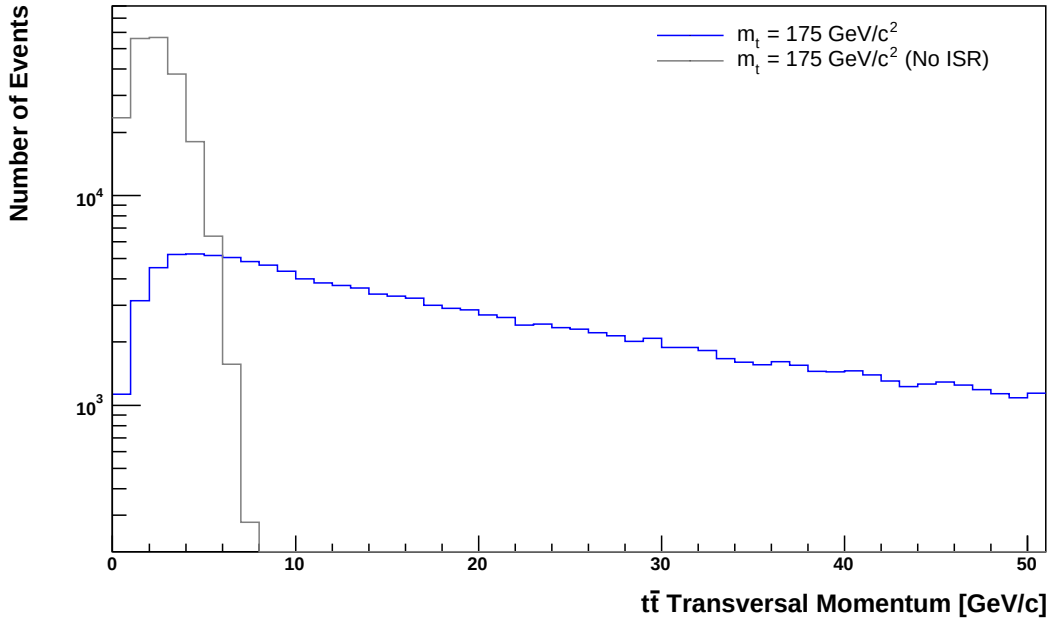

Figure 8.16: The influence of initial- and final-state radiation on L_{xy}

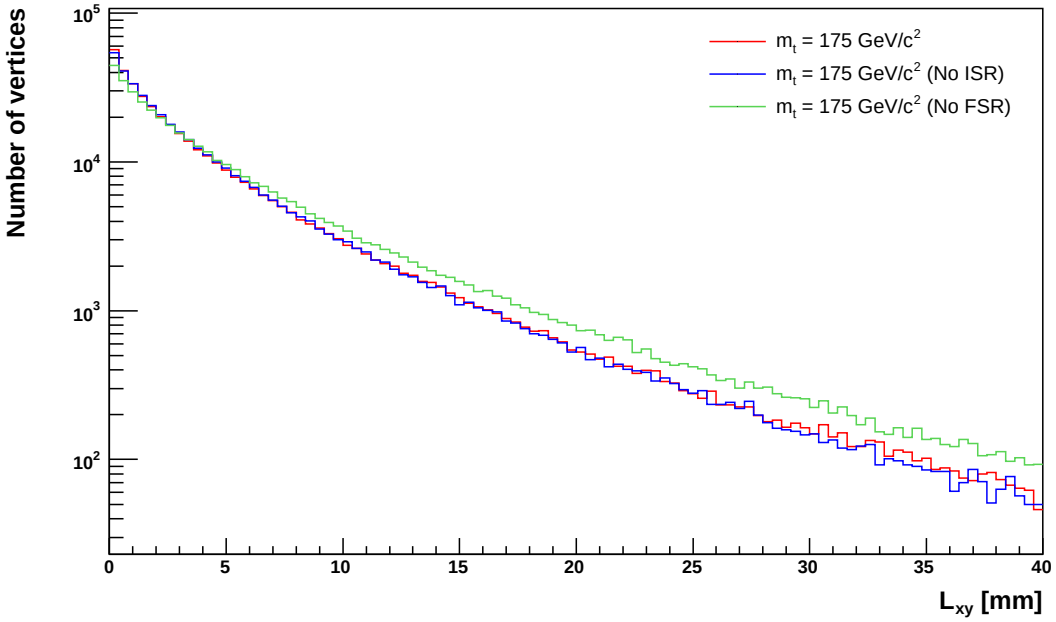

Table 8.10: $\langle L_{xy} \rangle$ fit parameters from the Pythia sample with initial-state radiation switched off ($m_t = 175$ GeV/c^2)

Sample	default	no ISR	Δm_t [GeV/c^2]
Mean L_{xy} over selected range [mm]			
Range (0, ∞)	4.505 ± 0.010	4.423 ± 0.010	—
Range (5, ∞)	11.698 ± 0.026	11.348 ± 0.024	1.8
Range (3, 20)	7.334 ± 0.010	7.276 ± 0.010	0.8
Range (5, 25)	9.988 ± 0.014	9.905 ± 0.014	—
Exponential fit over selected range [mm]			
Range (0,15)	3.451 ± 0.008	3.488 ± 0.008	—
Range (4,15)	4.758 ± 0.025	4.657 ± 0.024	—
Range (5,20)	5.283 ± 0.026	5.142 ± 0.025	1.1
Range (5,25)	5.515 ± 0.024	5.378 ± 0.023	1.1

Final-state radiation changes the fraction of bottom quark transverse momentum carried by the bottom hadron (this is illustrated in figure 8.17). Because of that a significant shift of top quark mass should be expected. Fit parameters obtained from modified Pythia sample are listed in table 8.11. The systematic error is again divided by 5.

Figure 8.17: Fraction of bottom quark p_{T} carried by the final bottom hadron. Comparison of samples with and without final-state radiation.

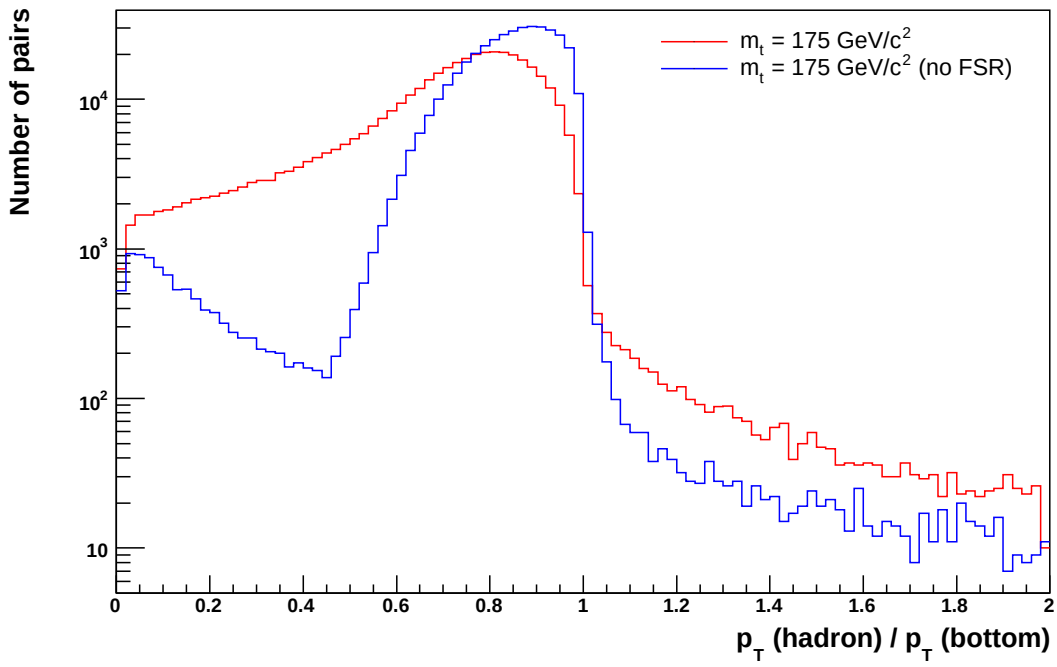

Because of that an additional study was performed on a sample from full simulation without final-state radiation (other settings were left the same as in the case of the default $m_t = 175$ GeV/c^2 sample). Fit parameters of both samples are compared in table 8.12. We take the slope of mass dependence obtained from full simulation for the calculation of systematic errors. These are significantly smaller than those from Pythia samples.

8.5.5 Jet Energy Scale

Jet energy is not used directly in this method of top quark measurement. Nevertheless it affects the way events are selected – the E_{T} cut on b-jets is of principal importance here. Therefore we studied effects that a change of this cut would bring about. We worked out the fit parameters for b-jet E_T cuts ranging from 15 to 35 GeV on the 4522 sample (with the largest

Table 8.11: $\langle L_{xy} \rangle$ fit parameters from the Pythia sample with final-state radiation switched off ($m_t = 175$ GeV/c^2)

Sample	default	no FSR	Δm_t [GeV/c^2]
Mean L_{xy} over selected range [mm]			
Range (0, ∞)	4.505 ± 0.010	5.422 ± 0.012	—
Range (5, ∞)	11.698 ± 0.026	12.379 ± 0.026	3.6
Range (3, 20)	7.334 ± 0.010	7.628 ± 0.010	4.0
Range (5, 25)	9.988 ± 0.014	10.292 ± 0.013	—
Exponential fit over selected range [mm]			
Range (0,15)	3.451 ± 0.008	4.126 ± 0.010	—
Range (4,15)	4.758 ± 0.025	5.227 ± 0.027	—
Range (5,20)	5.283 ± 0.026	5.755 ± 0.027	3.6
Range (5,25)	5.515 ± 0.024	6.028 ± 0.025	4.3

Table 8.12: $\langle L_{xy} \rangle$ fit parameters from the full simulation with final-state radiation switched off ($m_t = 175$ GeV/c^2)

Sample	default	no FSR	Δm_t [GeV/c^2]
Mean L_{xy} over selected range [mm]			
Range (0, ∞)	7.94 ± 0.30	8.56 ± 0.31	—
Range (5, ∞)	12.31 ± 0.46	13.11 ± 0.46	2.6
Range (3, 20)	7.72 ± 0.16	7.78 ± 0.16	< 1.4
Range (5, 25)	10.23 ± 0.22	10.47 ± 0.23	—
Exponential fit over selected range [mm]			
Range (0,15)	16.4 ± 2.1	11.9 ± 1.1	—
Range (4,15)	5.17 ± 0.50	4.49 ± 0.36	—
Range (5,20)	5.03 ± 0.36	5.00 ± 0.41	< 2.0
Range (5,25)	5.28 ± 0.34	5.52 ± 0.44	< 3.6

Figure 8.18: $\langle L_{xy} \rangle$ - fit parameters using different jet E_{T} cuts on the 4522 sample from Rome production

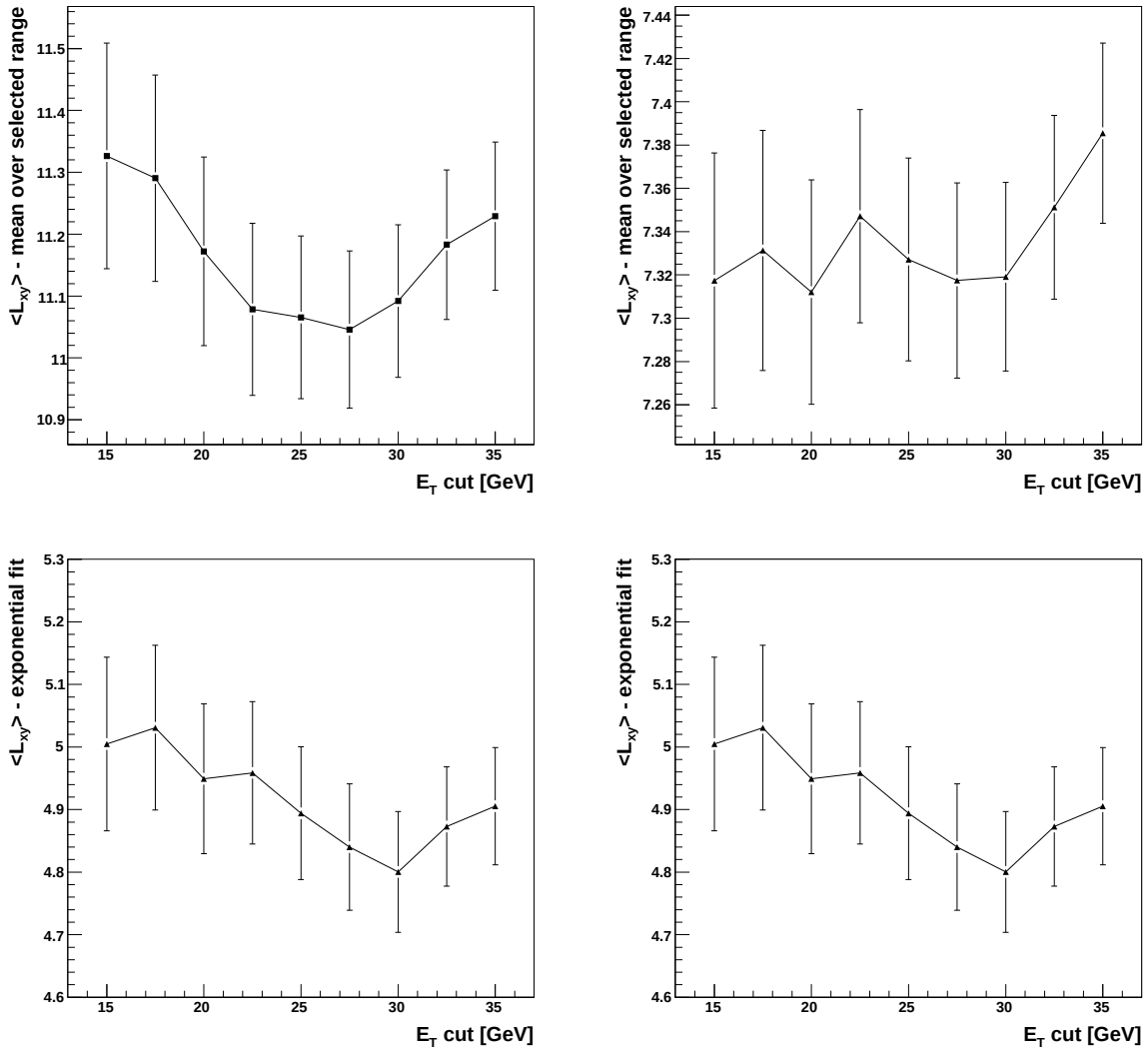

statistics) from Rome production. The results are plotted in figure 8.18. According to equation 4.6 we should count with the relative error of jet energy measurement of 2.5 GeV in this range of energies. If we take into account the error bars of individual points, the quantization seems impossible. A (very) naïve look at the plots indicates that the uncertainty probably is not larger than 2 GeV/c^2. Therefore we refer to [20] where the error associated with jet energy scale is small in comparison with other sources of systematic uncertainties.

Table 8.13: $\langle L_{xy} \rangle$ fit parameters from Rome production samples 4522 and 4321

Sample	4522	4321
Mean L_{xy} over selected range [mm]		
Range (0, ∞)	5.49 ± 0.06	5.33 ± 0.36
Range (5, ∞)	11.07 ± 0.13	12.42 ± 0.84
Range (3, 20)	7.33 ± 0.05	7.42 ± 0.30
Range (5, 25)	9.68 ± 0.07	10.27 ± 0.43
Exponential fit over selected range [mm]		
Range (0,15)	5.02 ± 0.06	3.56 ± 0.21
Range (4,15)	4.74 ± 0.12	3.26 ± 0.44
Range (5,20)	4.89 ± 0.11	4.24 ± 0.95
Range (5,25)	5.02 ± 0.10	5.12 ± 1.30

8.5.6 Background

The influence of background is negligible according to the authors of [20]. Although a check of their assumption would be very useful, our limited statistics did not make it possible for us to prove.

We list the fit parameters coming from the only background channel with a reasonable statistics, i.e. the 4321 sample (with leptonically decaying Z and two b jets) from the Rome production in table 8.13 and we compare them with the 4522 signal sample. With the exception of two rejected exponential parametrizations and the mean over range 5 to ∞ values are within the range of fit uncertainty.

If we take the shift in $\langle L_{xy} \rangle_5^\infty$ parameter and multiply it by the fraction of these events in real data with cuts applied on them, we get an estimated error due to this particular channel of 0.3 GeV/c^2. This can be safely neglected but there are more important channels that we did not investigate. A more detailed study could be useful here but probably the better approach to take is to look for selection criteria with better background rejection.

8.6 Uncertainty summary and outlook

In table 8.14 we summarize all studied sources of systematic and statistical uncertainties. We compare them with the results obtained by the authors of [20], the only detailed study of this method published at the moment. The systematic error was projected assuming its inverse square root dependence

Table 8.14: Uncertainties of the top quark measurement using mean transverse decay length method. In the case of final-state radiation we take results obtained from full simulation. Values are given in GeV/c^2.

Source	$\langle L_{xy}\rangle_5^\infty$	$\langle L_{xy}\rangle_3^{20}$	$\langle l_{xy}\rangle_5^{20}$	$\langle l_{xy}\rangle_5^{25}$	Reference [20]
Parton distributions	2.4	< 0.7	< 1.0	1.7	0.7
Bottom lifetime	1.8	2.0	2.1	2.0	1.3
Bottom fragmentation	< 0.7	< 0.7	< 1.1	< 0.9	1.2
Initial-state radiation	1.8	0.8	1.1	1.1	1.3
Final-state radiation	2.6	< 1.4	< 2.0	< 3.6	0.5
Jet energy scale	< 2.0?	< 2.0	< 2.0	< 2.0	0.2
Background	0?	0?	0?	0?	0
Total systematic error	< 4.8	< 3.4	< 4.0	< 5.1	2.4
Statistical error	7	7	10	13	–
Statistical error [10 fb^{-1}]	2.4	2.4	3.4	4.4	0.9
Total error [10 fb^{-1}]	5.4	4.2	5.2	6.7	2.5

on number of events.[9]

Total uncertainty expected for our best parameter $\langle L_{xy}\rangle_3^{20}$ after 10 fb^{-1} is 4.2 GeV/c^2 provided larger statistics from full simulation will allow us to determine the mass dependence of fit parameters with better precision. This precision may seem inferior to the precision claimed by the groups studying top quark measurement ($\sim$ 1.5 GeV/c^2) using kinematic reconstruction of 'lepton+jets' or 'dilepton' (and to some extent 'all-jets') channel. However this approach was studied for years by several groups and many sophisticated methods were developed for this purpose.

When the method described in this work gets more interest from physicists[10] bolder statements can be made – authors of [20] claim that the precision of $\sim$ 1.5 GeV/c^2 can be attained. Even repeating studies described in this work on larger amounts of data will probably allow us to reduce the estimation of systematic error coming from final-state radiation and jet energy scale (hopefully to values proposed by [20]). If better selection cuts will be applied (the signal efficiency could be significantly better if the selection of particles will be done in a more sophisticated way[11]) the statistical error

[9] Our $\sim$ 6500 events multiplied by the factor of 6.5 due to criteria loosening give about one ninth of 400,000 events expected for 10 fb^{-1} of integral luminosity.

[10] A group studying this topic emerges at the University of Dortmund at the moment [43] and Dimitrios Typaldos from the University of Birmingham is also investigating it. [36]

[11] At least other studies investigating the 'dilepton' channel claim higher efficiency.

will decrease, the negligibility of background (tacitly presumed here) can be proved and finally our selection criteria loosening can be avoided. As the correlation between $\langle L_{xy} \rangle_3^{20}$ and exponential fit parameters is not perfect, some likelihood combination of these results could allow an even better estimation of top quark mass. On the basis of these arguments we expect that a measurement of top quark mass with the uncertainty of ~ 2.5 GeV/c^2 can be made after 10 fb^{-1} of integrated luminosity with possible improvements in the future when measurements made at LHC will improve some parameters of B-physics and the statistical error will become negligible.

It should be possible to explain the laws of physics to a barmaid.

Albert Einstein

Chapter 9

Conclusion

In this thesis the decay length technique of top quark mass measurement and its application in the detector ATLAS using the 'dilepton' channel was investigated. Several parametrizations of the bottom hadron transverse decay length distributions were tested in order to find the one that will suffer from the lowest statistical and systematic uncertainties.

A rough study of severity was made for several sources of systematic uncertainty and a total uncertainty of 4.2 GeV/c^2 accessible after 10 fb^{-1} of data was estimated.

The signal efficiency and background rejection of standard selection criteria were also tested (the efficiency being ~ 1 % and the signal-to-background ratio being 5 to 1).

For these purposes data samples coming from three different sources were used:

- Samples from the official productions (Rome production, CSC11 production) were obtained either from web or using grid tools. They were used mainly for the selection-cut studies.
- Samples generated in Pythia for top quark masses from 150 to 200 GeV/c^2 were used for the studies of the kinematic properties of events, for theoretical prediction of the experimental distributions and for the estimating of systematic uncertainties.
- Samples with five different top quark masses generated using full simulation in ATLAS software release 11.0.4 were used for the determination of statistical error and for choosing the optimal parametrization. The sample generated without final-state radiation was used for the study of the error associated with FSR.

The CPU-intensive full simulation as well as a lot of other work was done at Golias farm in the Regional computing centre for particle physics [44] located in the Institute of Physics of the Academy of Sciences of the Czech Republic without which the analysis would be difficult as it would be almost impossible to get so much processor time elsewhere.

Bibliography

[1] S. Abachi *et al.* [D0 Collaboration], *Observation of the top quark*, Phys. Rev. Lett. **74** (1995) 2632 [arXiv:hep-ex/9503003].

[2] F. Abe *et al.* [CDF Collaboration], *Observation of top quark production in $\bar{p}p$ collisions*, Phys. Rev. Lett. **74** (1995) 2626 [arXiv:hep-ex/9503002].

[3] K. M. Black, *A precision measurement of the top quark mass*, PhD. thesis, Boston University, 2005.

[4] H. L. Lai *et al.* [CTEQ Collaboration], *Global QCD analysis of parton structure of the nucleon: CTEQ5 parton distributions*, Eur. Phys. J. C **12** (2000) 375 [arXiv:hep-ph/9903282].

[5] V. M. Abazov *et al.* [D0 Collaboration], *Evidence for production of single top quarks and first direct measurement of $|V_{tb}|$*, [arXiv:hep-ex/0612052].

[6] R. Bonciani, S. Catani, M. L. Mangano and P. Nason, *NLL resummation of the heavy-quark hadroproduction cross-section*, Nucl. Phys. B **529** (1998) 424 [arXiv:hep-ph/9801375].

[7] Z. Sullivan, *Understanding single-top-quark production and jets at hadron colliders*, Phys. Rev. D **70** (2004) 114012 [arXiv:hep-ph/0408049].

[8] J. Campbell and F. Tramontano, *Next-to-leading order corrections to W t production and decay*, Nucl. Phys. B **726** (2005) 109 [arXiv:hep-ph/0506289].

[9] J. Kvita, *Effects of top quark and W boson finite widths on the measurement of the top quark mass*, diploma thesis, Charles University, 2003.

[10] *Useful Diagrams of Top Signals and Backgrounds*, web page, http://www-d0.fnal.gov/Run2Physics/top/top_public_web_pages/top_feynman_diagrams.html.

[11] A. Abulencia *et al.* [CDF - Run II Collaboration], *Measurement of the Top Quark Mass in $p\bar{p}$ Collisions at $\sqrt{s} = 1.96$ TeV using the Decay Length Technique* [arXiv:hep-ex/0612061].

[12] V. Šimák *at al.*, *Reconstruction of top-antitop system from 2 leptons and 2 jets final states in experiment ATLAS*, ATL-COM-PHYS-99-073.

[13] V. M. Abazov *et al.* [D0 Collaboration], *Measurement of the top quark mass in the lepton + jets final state with the matrix element method*, Phys. Rev. D **74** (2006) 092005 [arXiv:hep-ex/0609053].

[14] A. Abulencia *et al.* [CDF Collaboration], *Top quark mass measurement using the template method in the lepton + jets channel at CDF II*, Phys. Rev. D **73** (2006) 032003 [arXiv:hep-ex/0510048].

[15] V. M. Abazov *et al.* [D0 Collaboration], *Measurement of the top quark mass in the dilepton channel*, [arXiv:hep-ex/0609056].

[16] A. Abulencia *et al.* [CDF Collaboration], *Top quark mass measurement from dilepton events at CDF II with the matrix-element method*, Phys. Rev. D **74** (2006) 032009 [arXiv:hep-ex/0605118].

[17] T. Aaltonen *et al.* [CDF Collaboration], *Measurement of the top-quark mass in all-hadronic decays in p anti-p collisions at CDF II*, [arXiv:hep-ex/0612026].

[18] A. Kharchilava, *Top mass determination in leptonic final states with J/psi*, Phys. Lett. B **476**, 73 (2000) [arXiv:hep-ph/9912320].

[19] I. Borjanović *et al.*, *Investigation of top mass measurements with the ATLAS detector at LHC*, Eur. Phys. J. C **39S2** (2005) 63 [arXiv:hep-ex/0403021].

[20] C. S. Hill, J. R. Incandela and J. M. Lamb, *A method for measurement of the top quark mass using the mean decay length of b hadrons in $t\bar{t}$ events*, Phys. Rev. D **71** (2005) 054029 [arXiv:hep-ex/0501043].

[21] E. Brubaker *et al.* [Tevatron Electroweak Working Group], *Combination of CDF and D0 results on the mass of the top quark*, [arXiv:hep-ex/0608032].

[22] *LHC Design Report*, CERN-2004-003-V-1,2,3, 2004.

[23] R. Barate *et al.* [LEP Working Group for Higgs boson searches], *Search for the standard model Higgs boson at LEP*, Phys. Lett. B **565** (2003) 61 [arXiv:hep-ex/0306033].

[24] *ATLAS detector and physics performance : Technical Design Report, 1, 2*, ATLAS-TDR-014,015, 1999.

[25] *ATLAS Inner Detector : Technical Design Report, 1,2*, ATLAS-TDR-004,005, 1997.

[26] Athena – The ATLAS Common Framework, Developer Guide, draft v8.0.

[27] *ATLAS Computing : Technical Design Report*, ATLAS-TDR-017, 2005.

[28] W. Lavrijsen, *The Athena Startup Kit*, web page, http://wlav.web.cern.ch/wlav/athena/athask/.

[29] The ATLAS Workbook, wiki page, https://uimon.cern.ch/twiki/bin/view/Atlas/WorkBook.

[30] K. A. Assamagan, *Tutorial on Athena and the Analysis EDM and Tools*, web page, http://www.usatlas.bnl.gov/PAT/AnalysisTutorial1103.html.

[31] WorkBookFullChain, wiki page, https://uimon.cern.ch/twiki/bin/view/Atlas/WorkBookFullChain.

[32] B. P. Kersevan, *$t\bar{t}$ Production at ATLAS and $t\bar{t}$ Monte Carlo Generators*, presented at International Workshop on Top Quark Physics, Coimbra, 2006.

[33] T. Sjostrand, S. Mrenna and P. Skands, *PYTHIA 6.4 physics and manual*, JHEP **0605** (2006) 026 [arXiv:hep-ph/0603175].

[34] K. A. Assamagan *et al.*, *Final report of the ATLAS AOD/ESD Definition Task Force*, ATL-SOFT-2004-006, 2004.

[35] AOD datasets at LBL website, http://phyweb.lbl.gov/AOD/10.0.1/.

[36] D. Typaldos, *Top mass measurement using B hadron decay length*, presented at ATLAS-UK Physics Meeting, September 2006.

[37] RomeBackgroundWiki web page,
https://uimon.cern.ch/twiki/bin/view/Atlas/RomeBackgroundWiki.

[38] H. Ma, *Di-boson studies with multi-lepton final states*, presented at ATLAS Physics Workshop 2005, Rome.

[39] RomeHiggsWiki web page,
https://uimon.cern.ch/twiki/bin/view/Atlas/RomeHiggsWiki.

[40] ZllJimmySample wiki web page,
https://uimon.cern.ch/twiki/bin/view/Atlas/ZllJimmySample/.

[41] W.-M. Yao *et al.*, *Review of Particle Physics*, J. Phys. G **33**, 1 (2006), available at http://pdg.lbl.gov/.

[42] E. Barberio *et al.* [Heavy Flavor Averaging Group (HFAG)], *Averages of b-hadron properties at the end of 2005*, [arXiv:hep-ex/0603003].

[43] J. Walbersloh, *Prospects of the decay length method for top quark measurement in ATLAS*, presented at T9 CSC Meeting, November 2006.

[44] Regional Computing Center for Particle Physics, web page,
http://www.particle.cz/farm/index.aspx?page=public.

Appendix A

Particles of the Standard Model

Table A.1: Fermions of the Standard Model [41] [21]

Name	Symbol	Charge	Mass (MeV)
electron	e	-1	0.5
electron neutrino	ν_e	0	$< 2 \times 10^{-6}$
muon	μ	-1	105.7
muon neutrino	ν_μ	0	< 0.19
tau	τ	-1	1777
tau neutrino	ν_τ	0	< 18.2
up quark	u	$\frac{2}{3}$	$1.5 \div 3.0$
down quark	d	$-\frac{1}{3}$	$3 \div 7$
charm quark	c	$\frac{2}{3}$	$1,250 \pm 90$
strange quark	s	$-\frac{1}{3}$	95 ± 25
top quark	t	$\frac{2}{3}$	$171,400 \pm 2,200$
bottom quark	b	$-\frac{1}{3}$	$4,200 \pm 70$

Table A.2: Gauge Bosons of the Standard Model [41]

Name	Symbol	Charge	Spin	Mass (GeV)
photon	γ	0	1	$< 6 \times 10^{-20}$
Z^0	Z^0	0	1	91.2
$W^\pm$	$W^\pm$	± 1	1	80.4
gluon	g	0	1	0
Higgs	H	0	0	> 114.4

Appendix B

Used Pythia Parameters

All statements are reproduced as they are used in the customized class inheriting from the TPythia6 C++ class in the ROOT framework. This class was used for generating our Pythia sample. Rewriting the settings in the language of Athena job options would be trivial (as seen for the process in C.1).

B.1 'Dilepton' Events Selection

```
SetMSEL(6);      // Heavy flavour process - ttbar only
SetMSTP(1, 3);   // Three generations of top-quarks (for sure)

/** Subprocesses **/
SetMSUB(81, 1);  // qq anihilation
SetMSUB(82, 1);  // gg fusion
SetMSUB(84, 0);  // g\gamma -> tt
SetMSUB(85, 0);  // \gamma\gamma -> tt

/** W decay channels **/
SetMDME(190, 1, 0);     // W -> dbar u
SetMDME(191, 1, 0);     // W -> dbar c
SetMDME(192, 1, 0);     // W -> dbar t (negligible)
SetMDME(193, 1, -1);    // W -> dbar t'(non-SM)
SetMDME(194, 1, 0);     // W -> sbar u
SetMDME(195, 1, 0);     // W -> sbar c
SetMDME(196, 1, 0);     // W -> sbar t (negligible)
SetMDME(197, 1, -1);    // W -> sbar t'(non-SM)
SetMDME(198, 1, 0);     // W -> bbar u
SetMDME(199, 1, 0);     // W -> bbar c
SetMDME(200, 1, 0);     // W -> bbar t (negligible)
SetMDME(201, 1, -1);    // W -> bbar t'(non-SM)
SetMDME(202, 1, -1);    // W -> b'bar u (non-SM)
SetMDME(203, 1, -1);    // W -> b'bar c (non-SM)
SetMDME(204, 1, -1);    // W -> b'bar t (non-SM)
SetMDME(205, 1, -1);    // W -> b'bar t'(non-SM)
SetMDME(206, 1, 1);     // W -> e nu_e (***)
SetMDME(207, 1, 1);     // W -> mu nu_mu (***)
SetMDME(208, 1, 0);     // W -> tau nu_tau (problems with tau-jets)
SetMDME(209, 1, -1);    // W -> tau' nu_tau' (non-SM)
```

B.2 Change of the Top Quark Mass

```
SetPMAS(6, 1, mass);    // The mass of the sixth quark (top)
```

B.3 Switching Off Initial-State Radiation

```
SetMSTP(61, 0);        // ISR off
```

B.4 Switching Off Final-State Radiation

```
SetMSTP(71, 0);        // FSR off
```

B.5 Change of the ϵ_b

```
SetPARJ(55, e_b);        // Peterson parameter to e_b
```

B.6 Selection of the PDF Set

```
SetMSTP(51, pdf);       // pdf = 8 (CTEQ5M1), 4 (GRV94M)
```

B.7 Change of the Bottom Hadron Lifetime

```
SetPMAS(Pycomp(kf), 4, tau * .299792458);
// Pycomp(kf) is the compressed particle code of the particle with PDG = kf
// Pythia accepts c*tau in mm, the input is lifetime in ps
```

Appendix C

Job Options – Full Simulation

C.1 Pythia Monte Carlo Generation

```
theApp.setup( MONTECARLO )

include( "PartPropSvc/PartPropSvc.py" )

theApp.Dlls  += [ "TruthExamples", "Pythia_i" ]
theApp.TopAlg = [ "Pythia" ]
theApp.ExtSvc += ["AtRndmGenSvc"]

MessageSvc = Service( "MessageSvc" )
MessageSvc.OutputLevel = ERROR

AtRndmGenSvc = Service( "AtRndmGenSvc" )
Pythia = Algorithm( "Pythia" )
Pythia.newScenario = FALSE
Pythia.OutputLevel = ERROR
Pythia.PythiaCommand = [ "pysubs msel 6" ]     # Top production

Pythia.PythiaCommand += [ "pysubs msub 1 0",    # ff->gamma/Z0
                          "pysubs msub 2 0",    # ff->W
                          "pysubs msub 83 0",   # qf->Qf
                          "pysubs msub 84 0",   # ggamma->QQ
                          "pysubs msub 85 0",   # 2gamma->QQ
                          "pysubs msub 142 0",  # ff->W'
                          "pysubs msub 81 1",   # ff->QQ
                          "pysubs msub 82 1",   # gg->QQ
                        ]
Pythia.PythiaCommand += [ "pypars mstp 1 3" ]   # Three generations of quarks

# W Decays
Pythia.PythiaCommand += [ "pydat3 mdme 190 1 0",
                          "pydat3 mdme 191 1 0",
                          "pydat3 mdme 192 1 0",
                          "pydat3 mdme 193 1 -1",
                          "pydat3 mdme 194 1 0",
                          "pydat3 mdme 195 1 0",
                          "pydat3 mdme 196 1 0",
                          "pydat3 mdme 197 1 -1",
                          "pydat3 mdme 198 1 0",
                          "pydat3 mdme 199 1 0",
                          "pydat3 mdme 200 1 0",
                          "pydat3 mdme 201 1 -1",
                          "pydat3 mdme 202 1 -1",
                          "pydat3 mdme 203 1 -1",
                          "pydat3 mdme 204 1 -1",
                          "pydat3 mdme 205 1 -1",
                          "pydat3 mdme 206 1 1",
                          "pydat3 mdme 207 1 1",
                          "pydat3 mdme 208 1 0",
```

```
                          "pydat3 mdme 209 1 -1",
                         ]


# PDF
Pythia.PythiaCommand += [ "pypars mstp 51 19070", "pypars mstp 52 2",
                          "pypars mstp 53 19070", "pypars mstp 54 2",
                          "pypars mstp 55 19070", "pypars mstp 56 2" ]

# Output
include( "AthenaPoolCnvSvc/WriteAthenaPool_jobOptions.py" )
theApp.Dlls   += [ "GeneratorObjectsAthenaPoolPoolCnv" ]
Stream1 = Algorithm( "Stream1" )
Stream1.ItemList += [ 'EventInfo#*', 'McEventCollection#*' ]

theApp.EvtMax = NEVENTS
Pythia.PythiaCommand += [ 'pydat2 pmas 6 1 ' + `TOPMASS` ]
Stream1.OutputFile = OUTFILE

# We use different random seed for each run of Pythia to get independent data files
from random import randint
seed1 = randint(1, 1000000000)
seed2 = randint(1, 1000000000)
seed3 = randint(1, 1000000000)

AtRndmGenSvc.Seeds = [ "PYTHIA " + `seed1` + " 90105060", "PYTHIA_INIT " + `seed2` + " " + `seed3` ]
```

C.2 Geant 4 Simulation

```
#--- Detector flags -----------------------------------------
from AthenaCommon.DetFlags import DetFlags
# - Select detectors
DetFlags.ID_setOn()
DetFlags.Calo_setOn()
DetFlags.Muon_setOn()
#
DetFlags.simulate.Truth_setOn()

#--- Simulation flags ---------------------------------------
from G4AtlasApps.SimFlags import SimFlags
SimFlags.import_Flags('atlas_flags')
SimFlags.SimLayout.set_Value('ATLAS-DC3-02')
SimFlags.KinematicsMode.set_Value('ReadGeneratedEvents')

theApp.EvtMax = 1000000 # -1 results in 3 due to G4Atlas_Sim.py

SimFlags.EvgenInput.set_Value( INFILE )
SimFlags.PersistencyHit.set_Value( OUTFILE )
include ( "G4Atlas_Sim.py" )
```

C.3 Digitization

```
PoolHitsInput = [ INFILE ]
PoolRDOOutput = OUTFILE
# Run through EvtMax events; if -1 run to end of file
EvtMax = -1

# Detector description
DetDescrVersion='ATLAS-DC3-02'

include ( "AtlasDigitization.py" )
include ( "GeneratorObjectsAthenaPool/GeneratorObjectsAthenaPool_joboptions.py" )

Stream1 = Algorithm( "Stream1" )
Stream1.ItemList+=["McEventCollection#*"]
```

C.4 Reconstruction (AOD)

```
# For AOD Production
doWriteESD = False
doWriteAOD = True

# Detector description
DetDescrVersion='ATLAS-DC3-02'

#number of Event to process (-1 is all)
EvtMax = -1
SkipEvents = 0

# suppress the production of ntuple and histogram files
doCBNT = False
doHist = False

# the input/output data files
PoolRDOInput = [ INFILE ]
PoolAODOutput = AODFILE
include( "RecExCommon_topOptions.py" )
```

Appendix D

AOD Contents (11.0.4)

```
<<<<<<<<<<<<<<<< Data Store Dump >>>>>>>>>>>>>>>>
StoreGateSvc(StoreGateSvc)::dump():
Found 1 proxy for ClassID 2101 (EventInfo):
 flags: (  valid, UNLOCKED,  reset) --- data:          0 --- key: McEventInfo
Found 8 proxies for ClassID 2806 (CaloClusterContainer):
 flags: (  valid, UNLOCKED,  reset) --- data:          0 --- key: CaloTopoCluster
 flags: (  valid, UNLOCKED,  reset) --- data:          0 --- key: CombinedCluster
 flags: (  valid, UNLOCKED,  reset) --- data:          0 --- key: EMTopoCluster
 flags: (  valid, UNLOCKED,  reset) --- data:          0 --- key: LArClusterEM
 flags: (  valid, UNLOCKED,  reset) --- data:          0 --- key: LArClusterEM33
 flags: (  valid, UNLOCKED,  reset) --- data:          0 --- key: LArClusterEM35
 flags: (  valid, UNLOCKED,  reset) --- data:          0 --- key: LArClusterEM37
 flags: (  valid, UNLOCKED,  reset) --- data:          0 --- key: LArClusterEMSofte
Found 1 proxy for ClassID 133273 (McEventCollection):
 flags: (  valid, UNLOCKED,  reset) --- data:          0 --- key: GEN_AOD
Found 1 proxy for ClassID 6771448 (LVL1_ROI):
 flags: (  valid, UNLOCKED,  reset) --- data:          0 --- key: LVL1_ROI
Found 1 proxy for ClassID 9327453 (VxContainer):
 flags: (  valid, UNLOCKED,  reset) --- data:          0 --- key: VxPrimaryCandidate
Found 1 proxy for ClassID 40774348 (AthenaAttributeList):
 flags: (  valid, UNLOCKED,  reset) --- data:  0xacadb98 --- key: Input
Found 4 proxies for ClassID 73891892 (MissingEtCalo):
 flags: (  valid, UNLOCKED,  reset) --- data:          0 --- key: MET_Base
 flags: (  valid, UNLOCKED,  reset) --- data:          0 --- key: MET_Calib
 flags: (  valid, UNLOCKED,  reset) --- data:          0 --- key: MET_Topo
 flags: (  valid, UNLOCKED,  reset) --- data:          0 --- key: MET_TopoBase
Found 1 proxy for ClassID 73891893 (MissingEtTruth):
 flags: (  valid, UNLOCKED,  reset) --- data:          0 --- key: MET_Truth
Found 12 proxies for ClassID 75817330 (MissingET):
 flags: (  valid, UNLOCKED,  reset) --- data:          0 --- key: AtlfastMissingEt
 flags: (  valid, UNLOCKED,  reset) --- data:          0 --- key: MET_Base
 flags: (  valid, UNLOCKED,  reset) --- data:          0 --- key: MET_Calib
 flags: (  valid, UNLOCKED,  reset) --- data:          0 --- key: MET_Cryo
 flags: (  valid, UNLOCKED,  reset) --- data:          0 --- key: MET_CryoCone
 flags: (  valid, UNLOCKED,  reset) --- data:          0 --- key: MET_Final
 flags: (  valid, UNLOCKED,  reset) --- data:          0 --- key: MET_Muon
 flags: (  valid, UNLOCKED,  reset) --- data:          0 --- key: MET_MuonBoy
 flags: (  valid, UNLOCKED,  reset) --- data:          0 --- key: MET_Topo
 flags: (  valid, UNLOCKED,  reset) --- data:          0 --- key: MET_TopoBase
 flags: (  valid, UNLOCKED,  reset) --- data:          0 --- key: MET_TopoObj
 flags: (  valid, UNLOCKED,  reset) --- data:          0 --- key: MET_Truth
Found 1 proxy for ClassID 77883132 (TruthParticleContainer):
 flags: (  valid, UNLOCKED,  reset) --- data:          0 --- key: SpclMC
Found 2 proxies for ClassID 83814411 ():
 flags: (  valid, UNLOCKED,  reset) --- data:  0xacadbf0 --- key: AthenaAttributeList/Input
 flags: (  valid, UNLOCKED,  reset) --- data:  0xacadb40 --- key: DataHeader/EventSelector
Found 1 proxy for ClassID 123529088 (CTP_Decision):
 flags: (  valid, UNLOCKED,  reset) --- data:          0 --- key: CTP_Decision
Found 1 proxy for ClassID 222376821 (DataHeader):
 flags: (  valid, UNLOCKED,  reset) --- data:  0xacadae8 --- key: EventSelector
Found 3 proxies for ClassID 1073853171 (MuonContainer):
 flags: (  valid, UNLOCKED,  reset) --- data:          0 --- key: AtlfastMuonCollection
```

```
 flags: (  valid, UNLOCKED,  reset) --- data:          0 --- key: MuidMuonCollection
 flags: (  valid, UNLOCKED,  reset) --- data:          0 --- key: StacoMuonCollection
Found 2 proxies for ClassID 1094973728 (PhotonContainer):
 flags: (  valid, UNLOCKED,  reset) --- data:          0 --- key: AtlfastPhotonCollection
 flags: (  valid, UNLOCKED,  reset) --- data:          0 --- key: PhotonCollection
Found 2 proxies for ClassID 1100041527 (TauJetContainer):
 flags: (  valid, UNLOCKED,  reset) --- data:          0 --- key: AtlfastTauJetContainer
 flags: (  valid, UNLOCKED,  reset) --- data:          0 --- key: TauJetCollection
Found 7 proxies for ClassID 1118613496 (ParticleJetContainer):
 flags: (  valid, UNLOCKED,  reset) --- data:          0 --- key: AtlfastParticleJetContainer
 flags: (  valid, UNLOCKED,  reset) --- data:          0 --- key: Cone4TowerParticleJets
 flags: (  valid, UNLOCKED,  reset) --- data:          0 --- key: Cone4TruthParticleJets
 flags: (  valid, UNLOCKED,  reset) --- data:          0 --- key: ConeTowerParticleJets
 flags: (  valid, UNLOCKED,  reset) --- data:          0 --- key: ConeTruthParticleJets
 flags: (  valid, UNLOCKED,  reset) --- data:          0 --- key: KtTowerParticleJets
 flags: (  valid, UNLOCKED,  reset) --- data:          0 --- key: KtTruthParticleJets
Found 2 proxies for ClassID 1163046103 (JetTagContainer):
 flags: (  valid, UNLOCKED,  reset) --- data:          0 --- key: AtlfastBJetContainer
 flags: (  valid, UNLOCKED,  reset) --- data:  0xb39cd60 --- key: BJetCollection
Found 1 proxy for ClassID 1235574503 (TrackRecordCollection):
 flags: (  valid, UNLOCKED,  reset) --- data:          0 --- key: MuonEntryRecordFilter
Found 1 proxy for ClassID 1314707306 (TrackParticleTruthCollection):
 flags: (  valid, UNLOCKED,  reset) --- data:          0 --- key: TrackParticleTruthCollection
Found 1 proxy for ClassID 1324108263 (INavigable4MomentumCollection):
 flags: (  valid, UNLOCKED,  reset) --- data:          0 --- key: TrackParticleCandidate
Found 8 proxies for ClassID 1334834594 (Rec::TrackParticleContainer):
 flags: (  valid, UNLOCKED,  reset) --- data:          0 --- key: MooreTrackParticles
 flags: (  valid, UNLOCKED,  reset) --- data:          0 --- key: MuTagTrackParticles
 flags: (  valid, UNLOCKED,  reset) --- data:          0 --- key: MuidCombTrackParticles
 flags: (  valid, UNLOCKED,  reset) --- data:          0 --- key: MuidExtrTrackParticles
 flags: (  valid, UNLOCKED,  reset) --- data:          0 --- key: MuonboyMuonSpectroOnlyTrackParticles
 flags: (  valid, UNLOCKED,  reset) --- data:          0 --- key: MuonboyTrackParticles
 flags: (  valid, UNLOCKED,  reset) --- data:          0 --- key: StacoTrackParticles
 flags: (  valid, UNLOCKED,  reset) --- data:          0 --- key: TrackParticleCandidate
Found 2 proxies for ClassID 1341992142 (ElectronContainer):
 flags: (  valid, UNLOCKED,  reset) --- data:          0 --- key: AtlfastElectronCollection
 flags: (  valid, UNLOCKED,  reset) --- data:          0 --- key: ElectronCollection
Found 18 proxies for ClassID 1667842791 (ParticleBaseContainer):
 flags: (  valid, UNLOCKED,  reset) --- data:          0 --- key: AtlfastBJetContainer
 flags: (  valid, UNLOCKED,  reset) --- data:          0 --- key: AtlfastElectronCollection
 flags: (  valid, UNLOCKED,  reset) --- data:          0 --- key: AtlfastMuonCollection
 flags: (  valid, UNLOCKED,  reset) --- data:          0 --- key: AtlfastParticleJetContainer
 flags: (  valid, UNLOCKED,  reset) --- data:          0 --- key: AtlfastPhotonCollection
 flags: (  valid, UNLOCKED,  reset) --- data:          0 --- key: AtlfastTauJetContainer
 flags: (  valid, UNLOCKED,  reset) --- data:          0 --- key: BJetCollection
 flags: (  valid, UNLOCKED,  reset) --- data:          0 --- key: Cone4TowerParticleJets
 flags: (  valid, UNLOCKED,  reset) --- data:          0 --- key: Cone4TruthParticleJets
 flags: (  valid, UNLOCKED,  reset) --- data:          0 --- key: ConeTowerParticleJets
 flags: (  valid, UNLOCKED,  reset) --- data:          0 --- key: ConeTruthParticleJets
 flags: (  valid, UNLOCKED,  reset) --- data:          0 --- key: ElectronCollection
 flags: (  valid, UNLOCKED,  reset) --- data:          0 --- key: KtTowerParticleJets
 flags: (  valid, UNLOCKED,  reset) --- data:          0 --- key: KtTruthParticleJets
 flags: (  valid, UNLOCKED,  reset) --- data:          0 --- key: MuidMuonCollection
 flags: (  valid, UNLOCKED,  reset) --- data:          0 --- key: PhotonCollection
 flags: (  valid, UNLOCKED,  reset) --- data:          0 --- key: StacoMuonCollection
 flags: (  valid, UNLOCKED,  reset) --- data:          0 --- key: TauJetCollection
<<<<<<<<<<<<<<<<<<<<<<<<<>>>>>>>>>>>>>>>>>>>>>>>>>
```